

THESIS FOR THE DEGREE OF PHILOSOPHY

**NEW APPROACHES FOR CHEMICAL  
ANALYSIS OF SINGLE CELLS AND VESICLES**

Johan Dunevall



Department of Chemistry and Chemical Engineering

Chalmers University of Technology

Göteborg, Sverige

2018

# **New Approaches for Chemical Analysis of Single Cells and Vesicles**

JOHAN DUNEVALL

ISBN: 978-91-7597-678-5

Löpnummer: 4359

© Johan Dunevall, 2018

Doktorsavhandlingar vid Chalmers Tekniska Högskola

ISSN 0346-718X

Department of Chemistry and Chemical Engineering

Chalmers University of Technology

SE-412 96 Göteborg

SVERIGE

Telephone: +46(0)31 772 1000

Cover picture:

Random-walk simulation of thousand particles in three dimensions.

Printed by Chalmers Reproservice

Göteborg, Sverige, 2018

# New Approaches for Chemical Analysis of Single Cells and Vesicles

Johan Dunevall

*Department of Chemistry and Chemical Engineering  
Chalmers University of Technology*

---

## Abstract

---

Exocytosis is the major cell-to-cell communication process in the nervous system, involving the conversion of an electrical signal (e.g. action potential) to a chemical one. Signaling molecules like neurotransmitters, hormones and/or peptides are stored in vesicles inside the cell. During exocytosis, calcium triggers the release of the vesicular cargo through SNARE-complex mediated fusion of the vesicles with the plasma (outer-membrane) of the cell. Consequently, a transient pore is formed through which the vesicular cargo is released into the extracellular space and is there able to interact with receptors of target cells. Most often, the pore closes again only allowing a fraction of the cargo to be released, so called partial release or kiss-and-run exocytosis. The extent of partial release is modulated by the intracellular calcium concentration, which can be regulated by the strength of the stimuli or with pharmaceuticals.

Despite the importance of this process and the efforts that have been done to resolve the fundamental regulatory mechanisms of exocytosis, much remains unknown. In order to gain understanding of how the amount of vesicular cargo released is regulated, information about the total vesicular cargo (quantal content) has to be obtained.

Until recently, no method aiming for quantification of the full quantal content existed. Our group has successfully developed an electrochemical method called vesicle impact electrochemical cytometry (VIEC) that allows direct quantification of the vesicular content in secretory granules as demonstrated with large dense-core granules from chromaffin and pheochromocytoma (PC12) cells.

Chromaffin cells of the adrenal medulla are the body's stress response output, and the best studied model system for exocytosis. The large-dense core vesicles of chromaffin cells contain a very important group of neurotransmitters and hormones, namely the catecholamines (e.g. dopamine, norepinephrine and epinephrine). The catecholamines are electroactive, and can

readily be oxidized at the surface of a polarized electrode to give away two electrons per molecule. By counting the number of electrons passed through the system (charge) and knowing the charge of one mole of electrons (Faraday's constant) the number of molecules can be quantified. In the intracellular or IVIEC method a conical nanotip carbon electrode is used to pierce into the cytosol of a living cell, allowing the vesicles to adsorb onto its surface. The vesicles burst open due to the electric field at the polarized electrode and the vesicular cargo is released towards the electrode surface and is oxidized, which allows the full content to be detected.

VIEC is an electrochemical method that potentially can be applied to study the quantal content of the electroactive vesicular content of other cell types like mast cells and blood platelets, that contain both histamine and serotonin.

**Keywords** Exocytosis, Catecholamines, Electrochemistry, Analytical chemistry, Chemistry

---

## List of Publications

---

- I. **Spatial Resolution of Single-Cell Exocytosis by Microwell-Based Individual Addressable Thin Film Ultramicroelectrode Arrays** J. Wang, R. Trouillon, J. Dunevall and A.G. Ewing. *Anal. Chem.*, 2014, 86 (9), 4515-4520

Took part in the fabrication of the device and was involved in the data analysis, reading and revising the paper.

- II. **Characterizing the Catecholamine Content of Single Mammalian Vesicles by Collision-Adsorption Events at an Electrode** J. Dunevall, H. Fathali, N. Najafinobar, J. Lovric, J. Wigström, A-S. Cans and A.G. Ewing. *J. Am. Chem. Soc.*, 2015, 137 (13), 4344-4346

Conceived the idea, planned and performed the experiments in consultation with A.G.E., analyzed the data and wrote the first draft of the paper, and coordinated all subsequent edits.

- III. **Quantitative Measurement of Transmitters in Individual Vesicles in the Cytoplasm of Single Cells with Nanotip Electrodes** X. Li, S. Majdi, J. Dunevall, H. Fathali and A.G. Ewing. *Angewandte Chemie Int. Ed.*, 2015, 54 (41), 11978-11982

Was involved in interpreting the data, outlining, reading and revising the paper.

- IV. **Lithographic Microfabrication of a 16-Electrode Array on a Probe Tip: Approaching the Nanometer Spatial Resolution of Exocytosis** J. Wigström, J. Dunevall, N. Najafinobar, J. Lovric, J. Wang, A.G. Ewing and A-S. Cans. *Anal. Chem.*, 2016, 88 (4), 2080-2087

Took part in the fabrication of the device, performed the Random-walk simulations, wrote the routine for the analysis of the data, and was involved in writing and revising the paper.

- V. **Excited Fluorophores Enhance the Opening of Vesicles at Electrode Surfaces in Vesicle Electrochemical Cytometry** N. Najafinobar, J. Lovric, S. Majdi, J. Dunevall, A-S Cans and A.G. Ewing. *Angewandte Chemie Int. Ed.*, 2016, 128 (48), 15305-15309

Conceptualized and performed the initial experiments together with N.N., and was involved in interpreting the data, reading and revising the paper.

- VI. **On the Mechanism of Electrochemical Vesicle Cytometry: Chromaffin Cell Vesicles and Liposomes** J. Lovric, N. Najafinobar, J. Dunevall, A. Oleinick, C. Amatore and A.G. Ewing. *Faraday Discussions*, 2016, 193, 65-79

Performed a minor part of the experiments. Was involved in the analysis and interpretation of the data, as well as reading and revising the manuscript.

- VII. **Nano Secondary Ion Mass Spectrometry Imaging of Dopamine Distribution Across Nanometer Vesicles** J. Lovric, J. Dunevall, A. Larsson, L. Ren, S. Andersson, A. Meibom, P. Malmberg, M.E. Kurczy and A.G. Ewing. *ACS nano*, 2016, 11, 3446-3455

Developed the analysis routine and analyzed the NanoSIMS data. Conducted the statistical evaluation together with J.L. of the NanoSIMS data and was involved in the statistical evaluation of the electrochemistry data. Wrote part of the manuscript.

- VIII. **DMSO Chemically Alters Cell Membranes to Slow Exocytosis and Increase the Fraction of Partial Transmitter Release** S. Majdi, N. Najafinobar, J. Dunevall, Jelena Lovric and A.G. Ewing. *ChemiBioChem*, 2017, 18 (19), 1898-1902

Was involved in interpreting the data, reading and revising the paper.

- IX. **Mechanistic Aspects of Vesicle Opening during Analysis with Vesicle Impact Electrochemical Cytometry** X. Li, J. Dunevall, L. Ren and A. G. Ewing. *Anal. Chem.*, 2017, 89 (17), 9416-9423

Involved in planning the experiments, interpreting the data, outlining the paper, reading and revising the paper.

---

## Related Publications not included in this thesis

---

**Two Modes of Exocytosis in an Artificial Cell** L.J. Mellander, M.E. Kurczy, N. Najafinobar, J. Dunevall, A.G. Ewing and A-S. Cans. *Scientific Reports*, 2014, 4, doi: 10.1038/srep03847

**Electrochemical Measurements of Optogenetically Stimulated Quantal Amine Release from Single Nerve Cell Varicosities in Drosophila Larvae** S. Majdi, E.C. Berglund, J. Dunevall, A.I. Oleinick, C. Amatore, D.E. Krantz and A.G. Ewing. *Angewandte Chemie Int. Ed.*, 2015, 127 (46), 13813-13816

**Using Single-Cell Amperometry to Reveal How Cisplatin Treatment Modulates the Release of Catecholamine Transmitters during Exocytosis** X. Li, J. Dunevall and A.G. Ewing. *Angewandte Chemie Int. Ed.*, 2016, 55 (31), 9041-9044

**Quantitative Chemical Measurements of Vesicular Transmitters with Electrochemical Cytometry** X. Li, J. Dunevall and A.G. Ewing. *Accounts of Chemical Research*, 2016, 49 (10), 2347-2354

**Cholesterol Alters the Dynamics of Release in Protein Independent Cell Models of Exocytosis** N. Najafinobar, L.J. Mellander, M.E. Kurczy, J. Dunevall, T.B. Angerer, J.S. Fletcher and A-S. Cans *Scientific Reports*, 2016, 6, doi: 10.1038/srep33702

**Osmotic Stress Reduces Vesicle Size while Keeping a Constant Neurotransmitter Concentration** H. Fathali, J. Dunevall, S. Majdi and A-S. Cans, *ACS Chemical Neuroscience* 2017, 8 (2), 368-375

**Vesicle Impact Electrochemical Cytometry Compared to Amperometric Exocytosis Measurements** J. Dunevall, S. Majdi, A. Larsson and A.G. Ewing *Current Opinion in Electrochemistry*, 2017

**Electrochemical Investigation of the Interaction Between Catecholamines and ATP** Z. Taleat, J. Estévez-Herrera, J. D. Machado, J. Dunevall, A. G. Ewing and R. Borges *Anal. Chem.*, 2017, *in press*



---

# Table of Contents

---

1	Introduction	1
1.1	The Nervous System	1
1.2	Cellular Communication	3
1.3	The Catecholamines: Neurotransmitters and Hormones	6
1.3.1	Dopamine	6
1.3.2	Norepinephrine	6
1.3.3	Epinephrine	7
1.3.4	Biosynthesis of Catecholamines	7
1.3.5	Deactivation and Metabolic Pathways	10
2	Exocytosis and cell Signaling	13
2.1	Cell Models	13
2.1.1	Chromaffin cells	13
2.1.2	PC12 cells	14
2.2	Exocytosis and the SNARE-Machinery	15
2.3	Secretory Vesicles	17
2.4	Regulatory Mechanisms	19
3	Electrochemical Theory	23
3.1	General Electrochemical Kinetics	23
3.2	Chronoamperometry	27
3.3	Cyclic Voltammetry	30
3.4	Connecting Chronoamperometry and Cyclic Voltammetry	33
4	Methods to Study Exocytosis	35
4.1	Background of Electrochemistry at Carbon Electrodes	35
4.1.1	Single Cell Amperometry	37
4.1.2	Vesicle Impact Electrochemical Cytometry	39

4.1.3	Fast-Scan Cyclic Voltammetry	40
4.1.4	Capacitance Measurements	41
4.2	Imaging Methods	43
4.2.1	Fluorescence Microscopy	43
4.2.2	Electron Microscopy	46
4.2.3	Imaging Mass Spectrometry	47
5	Simulations	49
5.1	Random-Walk	49
5.2	Finite Element Method	51
5.3	Conclusion of Simulation	52
6	Summary of Papers	53
7	Concluding Remarks and Future Outlook	57
8	Acknowledgements	61
9	References	63

---

# 1 Introduction

---

## 1.1 The Nervous System

The nervous system is constituted of two major parts, the *central nervous system* (CNS) and the *peripheral nervous system* (PNS). The CNS consist of the brain and the spinal cord and is surrounded by a highly selective semipermeable membrane called the *blood-brain barrier* (BBB). The function of the BBB is to supply the CNS with nutrition from the blood and keep, for example, neurotransmitters of the *cerebral spinal fluid* (CSF) separated from the rest of the body. The main function of the PNS is to act as a link between the CNS and the limbs and organs of the body. In humans, this is accomplished with 31 nerve pairs that protrude from the spinal cord. The PNS can further be divided into two sub-groups namely the *somatic-* (SNS) and the *autonomic nervous system* (ANS). The SNS is responsible for mediating conscious movements by connecting the brain and the skeletal muscles, but the SNS is also involved in sensation, such as, smell, vision, taste and pain. In contrast, the ANS that is responsible for the unconscious regulation of smooth muscles, cardiac rhythm and respiration. The ANS is comprised of the enteric nervous system, connecting to the gastrointestinal tract, the sympathetic, connecting for example the CNS with the adrenal gland via the splanchnic nerve as part of the body's fight-and-flight response. Lastly, the parasympathetic nervous system acts complimentary to the sympathetic nervous system by stimulating the body's rest-and-digest activities.<sup>1-3</sup>

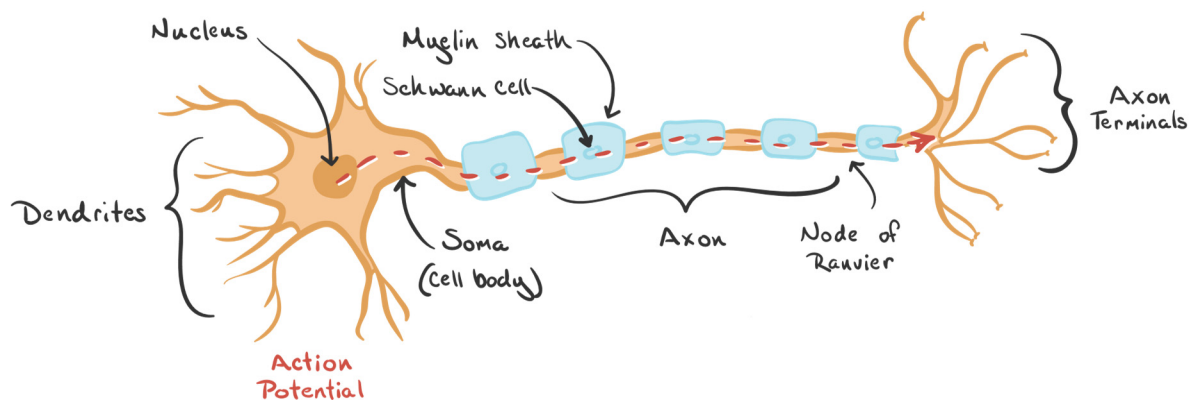


**Figure 1** A typical nerve cell is illustrated with the direction of the signal propagation shown as the **dotted red line**. The dendrites are usually receiving the electrical input which is integrated in the cell body (soma) that also contains the axon Hillock, the action potential is sent along the axon, which is shown together with the insulating myelin sheath. The action potential arrives at the axon terminals (boutons) and is triggering exocytosis, and the signal is converted to a chemical output.

The nervous system is made up of a variety of different cell types that can mainly be divided into *neurons* and *glial cells*. Figure 1 shows a typical diagram of a nerve cell surrounded by a special class of *glial cells* and indicating the basic process of signal transport via an action potential along the axon. The *neurons* are generally thought of as the main cell type in the nervous system, but are outnumbered by the glial cells by a 1:10 ratio (100 billion *neurons*: 1 trillion *glial cells* in the human brain). However, the *neurons* are the main actors for signal transduction and are responsible for what is called higher brain functions, such as, memory, judgement, and personality. The function of glial cells in the nervous system is mainly (but not exclusively) to support the neurons with physical support, nutrients, and electrical insulation of the axons, as well *house-keeping* of the CSF. The *oligodendrocytes* are a *glial cell* type, that is mainly responsible for the support and insulation of neurons by the formation of a *myelin sheath* around the axons in the CNS. In the PNS the insulating *myelin sheath* is made up of the *Schwann* cells. The *astrocytes* and *satellite* cells reconstitute the main energy reserve in the CNS and PNS, respectively, by the storage of glycogen and the production of lactate. The *astrocytes* also regulate the concentrations of ions in the CSF, and clear released neurotransmitters from the CSF by uptake. A last, but highly important cell type is the *microglial cell*. These cells act as a first line of immune defense against pathogens, but are also responsible for the clearance of dead cells in the CNS.<sup>1-3</sup>

## 1.2 Cellular Communication

The cell-to-cell communication in the nervous system is mainly about the inter-conversion of electrical and chemical signals. A chemical signal in form of the release of hormones or neurotransmitters acts on a target cell by binding to specific receptors at its surface. This receptor-ligand interaction (the neurotransmitter or hormone is the ligand) can either increase or decrease the probability of the target cell to propagate the signal forward (firing an action potential). If the ligand-receptor interaction causes an increase the membrane potential, the ligand is said to have an *excitatory* effect and if it causes a decrease, it is said by inhibitory. There are two main types of ligand-gated receptors or channels, the first is the *metabotropic* receptors including the receptors from the *G protein-coupled receptor* (GPCR) family and the *tyrosine kinase* family. The *metabotropic* receptors mainly act by the production of secondary messengers, like *cyclic AMP* (cAMP) and *inositol 1,4,5-trisphosphate* (IP<sub>3</sub>), which causes secondary effects such as *phosphorylation* of proteins by the activation of *protein kinases* (PKA and PKC). In contrast to the *metabotropic* receptors, in members of the *ionotropic* receptors, the receptor (gating-unit) is directly linked to the ion channel and can in a direct way regulate the opening and closing of the channel. A wide variety of receptors exists throughout the body that are responsible for different tasks; In addition to the two previously described receptor types, a third type of receptor that is highly important for cellular communication exists, namely the voltage-gated channel receptors. The voltage-gated channels are, as the name implies, use a voltage-sensing unit to regulate the opening and closing of an ion channel, various version exists like for example K<sup>+</sup>, Na<sup>+</sup> an Ca<sup>++</sup> channels, which will be describe further in the text that follows.<sup>1-3</sup>

In neurons and neuroendocrine cells, the cytosol contains high concentration of K<sup>+</sup> and low concentration of Na<sup>+</sup> compared to the extracellular solution. This concentration difference between the two sides of the cellular membrane give rise to a potential difference across the membrane, that can be defined according to *Nernst* equation. The contribution of Na<sup>+</sup> to the resting potential for a neuroendocrine cell like a chromaffin cell can be described as following.

$$E_{Na^+} = \frac{RT}{F} \ln \left( \frac{[Na^+]_o}{[Na^+]_i} \right) = 27 \text{ mV} \ln \left( \frac{[150]}{[55]} \right) = +73 \text{ mV} \quad \text{Eq. 1}$$

Where *R* is the *general gas constant*, and *T* is the absolute temperature (310K, 37°C) and *F* is the *Faraday* constant. The contribution of Na<sup>+</sup> ion to the resting membrane potential is around +73 mV, but other ions likes K<sup>+</sup> and Cl<sup>-</sup> present at high concentrations around the membrane also significantly influence the membrane potential. Additionally, there is a continuous exchange of ions across the membrane, in the form of a steady Na<sup>+</sup> influx balanced by a steady K<sup>+</sup> efflux.

The rate of the flux is a function of the *permeability* ( $P$ ) of the ion across the cell membrane and its concentration. Both the contribution from individual ionic species and its *permeability* are accounted for in an extended form of the *Nernst* equation, called the *Goldman* equation.

$$V_m = \frac{RT}{F} \ln \left( \frac{P_{Na^+}[Na^+]_o + P_{K^+}[K^+]_o + P_{Cl^-}[Cl^-]_o}{P_{Na^+}[Na^+]_i + P_{K^+}[K^+]_i + P_{Cl^-}[Cl^-]_i} \right) \quad \text{Eq. 2}$$

Here,  $V_m$  is the membrane potential and all the other components are as described previously. The *permeability* across the membrane can rapidly be altered by the activation of ion channels that are capable of selectively control the flux of ions along a concentration gradient. This activation can either be ligand-gated (*metabotropic* and *ionotropic*) or voltage-gated.

Voltage-gated ion channels have a special role during the firing of an *action-potential* (AP); an AP is the generation and/or the propagation of an electrical signal within the cell (Figure 2). The cell takes a lot of inputs from neighboring cells usually through the dendrites for a typical neuronal cell. The input can either be *excitatory* or *inhibitory* meaning that the membrane potential ( $V_m$ ) is increased (*depolarized*) or decreased (*repolarized*), respectively. If the  $V_m$  exceeds the *threshold* potential (usually around  $-55 \text{ mV}$ , but differences exist between cell types) an AP is fired. In the case of a neuron, the AP is initiated at the *axon Hillock* - region of the soma (cell body) that is attached to the axon and is enriched with voltage-gated  $K^+$  and  $Na^+$  channels. Once the *threshold* potential is exceeded the voltage-gated  $Na^+$  channels open causing an influx of  $Na^+$  into the cytosol. This result in a sharp rise in  $V_m$  with a peaking around  $+40 \text{ mV}$ . However, the voltage-gated  $Na^+$  ions are only open for a short period of time before they are inactivated by the closure of an inactivation gate and thus become impermeable. During the depolarization process, voltage-gated  $K^+$  channels also open, after a delay time relative to the  $Na^+$  channels. Opening of the  $K^+$  channels cause an efflux of  $K^+$  from the cytosol to the extracellular space that balances the influx of  $Na^+$ . Since, the  $K^+$  channels are slower in responding and lack the inactivation gate they do not close until close until the  $V_m$  is more negative than the resting potential, which then causes a hyperpolarization of the cell. Once all channels are closed, the continued exchange of  $Na^+$  and  $K^+$  via the  $Na^+/K^+$ -ATPase-driven pump becomes the dominant, restoring the membrane potential to its resting potential.

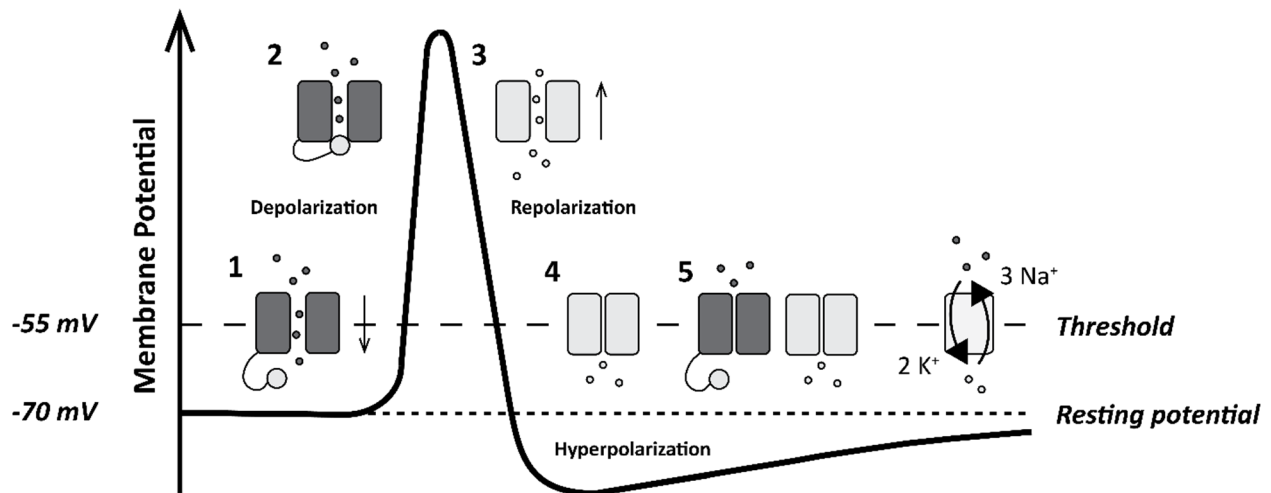


**Figure 2** A schematic image of the action potential is shown broken up in five steps. **1**, once the threshold is exceeded the voltage-gated Na<sup>+</sup> channels opens causing an influx of sodium ions resulting in a sharp rise in membrane potential (depolarization). **2**, The voltage-gated Na<sup>+</sup> channel rapidly becomes inactivated, and the membrane potential stops increasing. **3**, the voltage-gated K<sup>+</sup> is also activated but are slower in opening than the Na<sup>+</sup> channels, causing an efflux of potassium ions causing the membrane potential to decrease (repolarization). **4**, the voltage-gated K<sup>+</sup> do not close until the membrane potential has become more negative than the resting potential causing hyperpolarization. **5**, Once the potential has become lower than the threshold potential the voltage-gated Na<sup>+</sup> is restored to its original close state, and then the K<sup>+</sup>-channels also is closed again the resting membrane potential is restored by the continuous activity of the Na<sup>+</sup>/K<sup>+</sup>-ATPase pump.

The propagation of an electrical signal within the cell is carried out by sequential depolarization along the axon. Once an AP is started, the local membrane potential initiates continued downstream depolarization causing the propagation of the AP; the directionality is maintained owing to the *hyperpolarization* of the cell membrane, called the relative refractory period. During the relative refractory period, the probability for a new AP to fire in the same region is low due to the highly negative membrane potential (*hyperpolarization*). The rate of AP propagation along an axon can be significantly increased by the formation of nodes, places of conductivity with the solution in between insulating regions. These so-called *nodes of Ranvier* are separated by insulating regions of *myelin sheath* that are formed by *oligodendrocytes* (CNS) and *Schwann cells* (PNS). The insulation allows the AP to *jump* spatial intervals of about 1  $\mu\text{m}$  and is caused by movement of ions inside the axon along the electrical field, so called saltatory conduction. The saltatory conduction facilitates the conduction rate of the AP along an axon up to 100 m/s, which significantly speeds up the communication process. Finally, the arrival of an AP to the synapse (for example) triggers the opening of voltage-gated Ca<sup>++</sup> channels, which then causes an influx of Ca<sup>++</sup> and subsequently initiates the vesicle fusion and the process of *exocytosis*.<sup>1-4</sup>

## 1.3 The Catecholamines: Neurotransmitters and Hormones

### 1.3.1 Dopamine

Dopamine is the precursor of both norepinephrine and epinephrine, but it is also both a hormone and a neurotransmitter in its own right. The discovery of dopamine as a neurotransmitter of the CNS was made by Arvid Carlsson in the late 1950's, and in 2000 he was awarded the Nobel Prize in physiology for his work on dopamine mediated signal transduction in the CNS.<sup>5,6</sup> In the CNS, dopamine is involved in reward-motivation behavior and strongly associated with addictions. Many addictive drugs like for example cocaine and amphetamine increase the tonic (basal) levels of extracellular dopamine in the brain.<sup>7-9</sup> Dopamine is mainly acting as an inhibitory transmitter by decreasing the excitability of affected neurons. It appears to be mainly released through volume transmission (into the extracellular space rather than in synapses), which has led some to describe its action as neuromodulatory.<sup>10</sup> It is also important in locomotor activity, which is important in the affects observed during the loss of dopaminergic neurons in the *substantia nigra* related to *Parkinson's disease*.<sup>11,12</sup> More recently, biphasic changes of dopamine transmission have been shown to cause hyperkinesia during the early stages and hypokinetic movements during the late stages of, of *Huntington's disease*.<sup>13</sup>

### 1.3.2 Norepinephrine

In 1945, Ulf von Euler reported on the physiological effects of intravenously injection of isolated norepinephrine.<sup>14</sup> He later demonstrated that norepinephrine is produced, stored in vesicles, and released from nerve endings.<sup>15</sup> For this work, he was awarded the Nobel Prize in 1970. Norepinephrine also called noradrenaline is the precursor to epinephrine, but also acts as a hormone and a neurotransmitter on its own. In the endocrine, system norepinephrine is released from the adrenal medulla and enters the blood stream. It primarily interacts with  $\alpha_1$ -adrenergic receptors to cause vasoconstriction and to increase blood pressure, but does not increase cardiac output as a hormone. However, norepinephrine released from the postganglionic neurons that innervate the heart muscles acts as a transmitter and increases cardiac output by regulating contractility and heart rate.<sup>15,17</sup> In the central nervous system, norepinephrine function as a transmitter released by neurons located in the *locus coeruleus*, a nucleus of the brain stem with many complex modulatory functions. Although, these adrenergic neurons are relatively few, they project diffusely throughout the cortex, cerebellum, and spinal cord.<sup>18</sup>

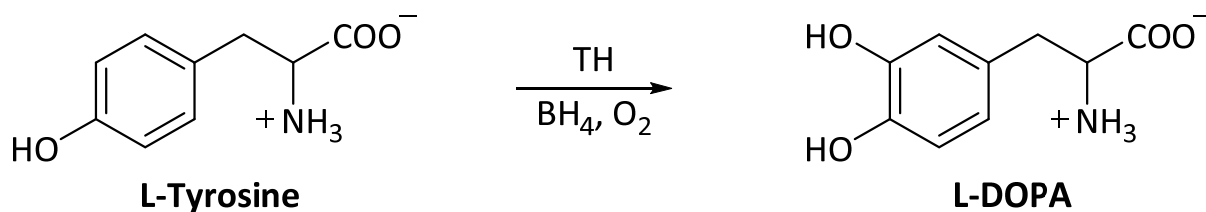
### 1.3.3 Epinephrine

Epinephrine, also called adrenaline, is a hormone and neurotransmitter produced in chromaffin cells of the adrenal medulla and in some adrenergic neurons. The physiological effects of epinephrine were the first to be described in the late 1800's, but its role as a neurotransmitter was not found until 1974.<sup>19</sup> Epinephrine, similarly to norepinephrine, acts on both the  $\alpha$ -adrenergic and  $\beta$ -adrenergic receptors, in a complex, tissue specific and concentration dependent manner. It can both act as vasoconstrictor through activation of  $\alpha_1$ -receptors and vasodilator by mediating  $\beta_2$ -receptors. Since,  $\beta_2$ -receptors have higher affinity for epinephrine than  $\alpha_1$ -receptors, vasodilation predominates at low levels, whereas at high levels vasoconstriction dominates. Epinephrine is also responsible for regulating of the cardiac output, such as, heart rate and contractility, through the interaction with  $\beta_2$ -receptors.<sup>20</sup> In addition, it also mobilizes energy by inducing glycogenolysis and lipolysis in the liver.<sup>21</sup> It is also used therapeutically as a bronchodilator, increasing the airflow to the lungs in the case of an anaphylactic shock.<sup>22</sup>

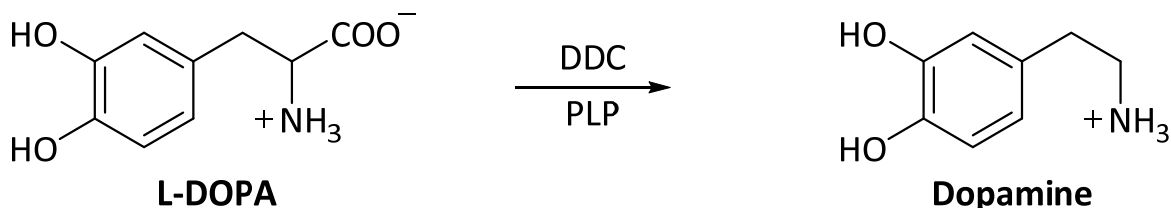
### 1.3.4 Biosynthesis of Catecholamines

The catecholamines, a group of neurotransmitters and hormones including norepinephrine, epinephrine and dopamine are all synthesized from the essential amino acid tyrosine. The biosynthetic pathway from tyrosine to epinephrine consists of four enzymes tyrosine hydroxylase, DOPA decarboxylase also known as aromatic amino acid decarboxylase, dopamine- $\beta$ -hydroxylase and phenylethanolamine N-methyltransferase.<sup>3</sup>

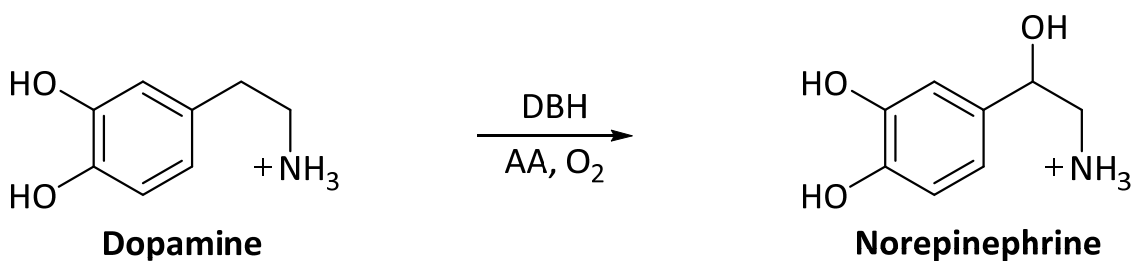
The enzyme tyrosine hydroxylase (TH) is a mixed-function oxidase that is found in all cells producing catecholamines. TH uses molecular oxygen ( $O_2$ ) and biopterin ( $BH_4$ ) as co-factors to catalyze the addition of a hydroxyl group in the meta position of tyrosine to form 3,4-dihydroxy-L-phenylalanine (L-DOPA). It is also the rate-limiting enzyme of catecholamine biosynthesis; TH receives feedback inhibition by competitive binding between biopterin and the downstream products dopamine, norepinephrine, and epinephrine. This makes TH a highly important enzyme for catecholamine homeostasis in the cell.<sup>23,24</sup>



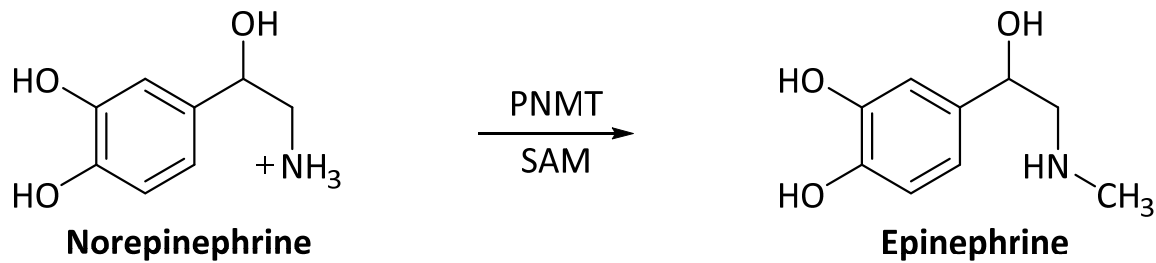
DOPA decarboxylase (DDC) is a pyridoxine-dependent lyase enzyme responsible for the decarboxylation of L-DOPA to dopamine (DA). The high  $V_{max}$  and low  $K_m$  of DDC with respect to L-DOPA facilitates large conversion rates, which allows the rate-limiting enzyme of the dopamine synthesis TH to be effectively by-passed by increasing the cytosolic L-DOPA levels (used in **paper III, VII and IX**). DDC is also capable of decarboxylating other aromatic amino acids, such as, 5-hydroxytryptophan, the precursor to serotonin and therefore is also often referred to as aromatic amino acid decarboxylase (AADC). The DDC is found in a wide range of cells and tissues like, for example, adrenergic, dopaminergic and serotonergic neurons as well as non-neuronal tissue like blood vessels and kidney.<sup>25</sup>



Similar to TH, dopamine- $\beta$ -hydroxylase (DBH) is a mixed-function oxidase that uses molecular oxygen as a cofactor to introduce a hydroxyl group at the  $\beta$ -carbon on the side chain of DA. The DBH enzyme exists both as a dimer and a tetramer with two  $\text{Cu}^{++}$  ions per domain. This facilitates the electron transfer in the reaction and uses ascorbate as the electron donor. Hence, DBH activity is sensitive to copper chelators, such as diethyldithiocarbamate, that are potent inhibitors of the enzyme. The enzyme is mostly found as a membrane bound protein and to a smaller extent as a soluble protein inside of catecholamine containing large dense-core vesicles. Dopamine must be loaded into the vesicles from the cytosol by the vesicle monoamine transporter (VMAT) to be converted to norepinephrine. DBH is to a certain degree co-released together with norepinephrine and epinephrine, mainly from the chromaffin cells of the adrenal medulla and is therefore found in plasma.<sup>26-28</sup>



The enzyme phenylethanolamine *N*-methyltransferase (PNMT) is found in a small group of adrenergic neurons in the amygdala and the retina, but is mostly found in the cells of the adrenal medulla. PNMT catalyzes the conversion of norepinephrine to epinephrine by the transfer of a methyl group from *S*-adenosyl methionine (SAM) to the nitrogen of norepinephrine, resulting in a secondary amine. PNMT, in contrast to DBH, is located in the cytosol of the cell, and consequently biosynthesized norepinephrine has to leave the vesicle in order to be converted to epinephrine. The epinephrine is subsequently pumped back into the vesicles in order to be released. The activity of PNMT in the cells of the adrenal medulla is modulated at the transcriptional level by glucocorticoid hormones released from the adrenal cortex.<sup>29-32</sup>



### 1.3.5 Deactivation and Metabolic Pathways

In contrast to the synthesis of catecholamines that has one major pathway, catecholamine metabolism has several different pathways depending on which catecholamine and what region of the body, shown in Figure 3. Norepinephrine and epinephrine are metabolized to 3-methoxy-4-hydroxy-phenylglycol (MHPG) by two different pathways called the adrenalmedullary and the sympathoneuronal pathway.<sup>33,34</sup> The sympathoneuronal pathway is the major pathway for production of catecholamine metabolites. This is mainly because the major deactivation pathway of norepinephrine following release is by reuptake and storage. Consequently, the majority of metabolism takes place in adrenergic neurons or in surrounding cells, like for example in Schwann cells.<sup>35</sup> The first step of the sympathoneuronal pathway is an oxidative deamination reaction of norepinephrine to 3,4-dihydroxyphenylglycolaldehyde (DOPEGAL) catalyzed by monoamine oxidase (MAO). MAO is an enzyme containing a covalently bound FAD cofactor and is located in the outer membrane of the mitochondria in many cell types.<sup>36</sup> The second step, is a reduction of DOPEGAL to 3,4-dihydroxyphenylglycol (DHPG) that potentially can be catalyzed by two enzymes, aldehyde reductase (ALR) and aldose reductase (AR). *In vitro* studies of ALR and AR have shown that AR has larger activity for the conversion of DOPEGAL to DHPG than ALR, but also that it exists at higher abundance in superior cervical ganglionic (SCG), heart, and adrenal medulla tissues of rat as well as in human sympathetic ganglia.<sup>37,38</sup> The third step is the conversion of DHPG to 3-methoxy-4-hydroxy-phenylglycol (MHPG), which involves the introduction of a methyl group at the third position of the catechol ring. The methyl group is donated by S-adenosyl methionine (SAM) and the reaction is catalyzed by the enzyme catechol-O-methyltransferase (COMT). COMT is a magnesium-dependent enzyme that is most abundant in the liver, pancreas, and the pituitary glands but does also exists in different brain areas, peripheral nerves, and ganglia, as well as in blood vessels.<sup>39</sup> There are two isoforms of COMT, a membrane-bound (MB-COMT) and a soluble (S-COMT).<sup>40</sup> The MB-COMT is predominantly expressed in brain neurons, while S-COMT is expressed in other tissues, such as liver, blood, and kidney.<sup>41,42</sup>

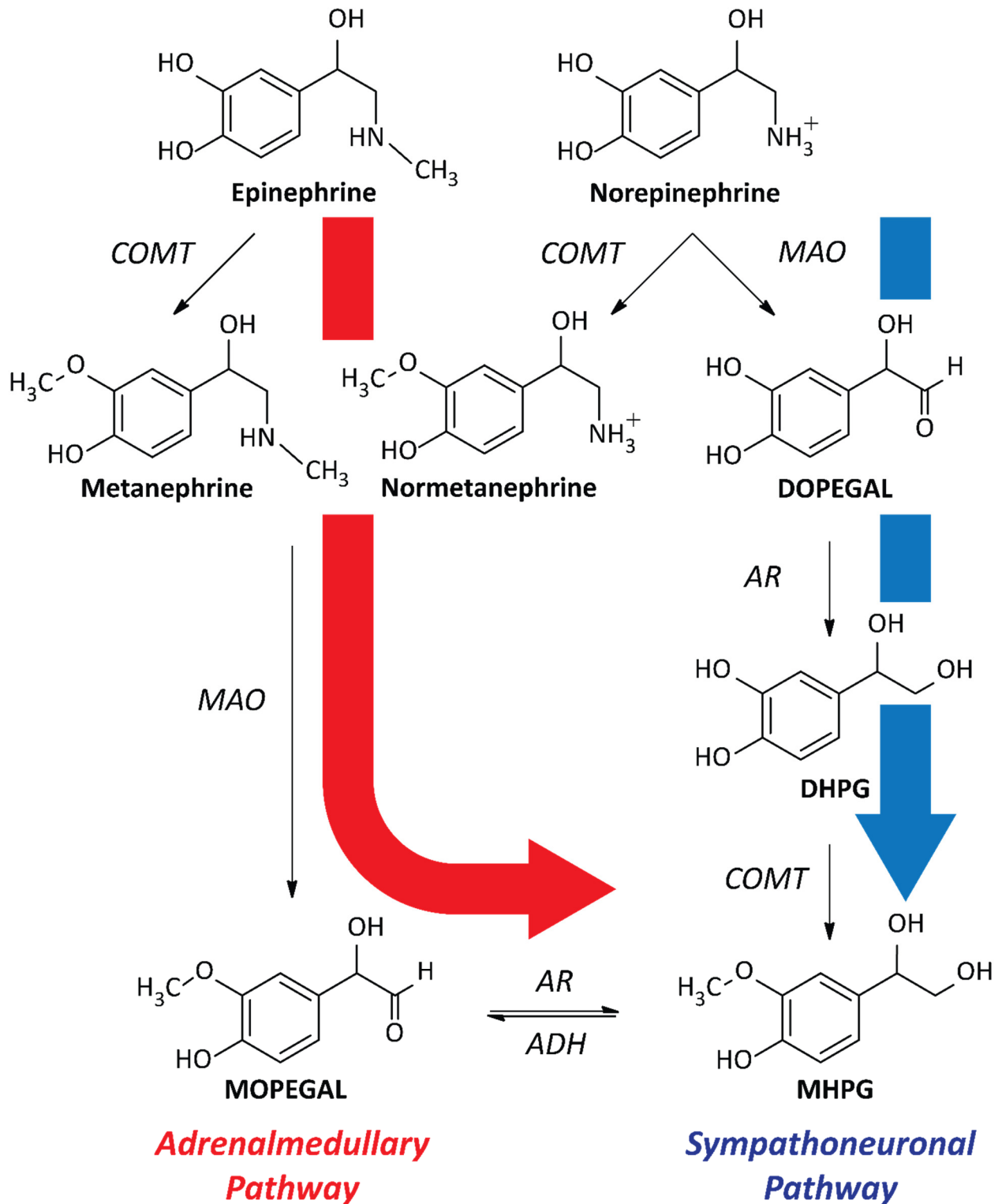


**Figure 3** A schematic of the two major pathways of norepinephrine and epinephrine metabolism in the endocrine system (*Adrenalmedullary pathway*) and in the nervous system (*Sympathoneuronal pathway*).

The metabolite MHPG is also produced to a lesser extent by another pathway called the adrenalmedullary pathway. The adrenalmedullary pathway is the main metabolic pathway for norepinephrine and epinephrine released into the blood stream by the chromaffin cells of the adrenal medulla. The pathway involves the conversion of norepinephrine and epinephrine to normetanephrine and metanephrine, respectively. This conversion involves a methylation reaction catalyzed by the enzyme COMT. Subsequently, 3-methoxy-4-hydroxyphenylglycoaldehyde (MOPEGAL) is produced by the MAO assisted deamination of normetanephrine and metanephrine. MOPEGAL is later reduced by AR and/or ALR to MHPG. MHPG is the main metabolite found in the systemic circulation (blood and cerebellum spinal fluid (CSF)), but the major metabolite excreted in urine is vanillylmandelic acid (VMA). VMA is produced from MHPG in the liver in two-steps via the MOPEGAL intermediate by the enzymes alcohol dehydrogenase (ADH) and aldehyde dehydrogenase (ALDH).<sup>33,34</sup>

A third pathway also exists, which involves the production of mainly MHPG-sulfate but also other sulfate conjugated norepinephrine metabolites. These reactions take place in mesenteric organs (gastrointestinal tract, pancreas and spleen), which contain high concentrations of the sulfotransferase enzymes (SULTs). The sulfate-conjugated metabolites leave the mesenteric tissue to enter the systemic circulation and eventually are excreted in urine, similar to VMA.<sup>33,34</sup>

Dopamine has a similar metabolic pathway to norepinephrine with an oxidative deamination facilitated by MAO to form the aldehyde adduct, 3,4-dihydroxyphenylacetaldehyde (DOPAL). Instead of the formation of a glycerol as a second step as for norepinephrine, the carboxylic acid 3,4-dihydroxyphenylacetic acid (DOPAC) is produced by an aldehyde dehydrogenase (ALDH) catalyzed oxidation of DOPAL. In the last step homovanillic acid (HVA) is produced by methylation of DOPAC by COMT.<sup>34</sup>

---

## 2 Exocytosis and cell Signaling

---

### 2.1 Cell Models

#### 2.1.1 Chromaffin cells

Chromaffin cells are a type of neuroendocrine cell localized to the medulla of the adrenal gland. The chromaffin cells form a sympathetic paraganglion that receives excitatory cholinergic inputs from the splanchnic nerve. Acetylcholine released from the splanchnic nerve terminals interacts with muscarinic (GPCR) and nicotinic (ionotropic) receptors and induces the depolarization of the cells, causing an influx of  $\text{Ca}^{++}$  through activated voltage-gated calcium channels. The increased levels of cytosolic  $\text{Ca}^{++}$  then triggers the release of small molecular species, like epinephrine, norepinephrine, and ATP, as well as bioactive peptides and larger hormones from large-dense core vesicles (LDCVs).

The chromaffin cells are relatively large spherical shaped cells that can be isolated from many different sources, such as, rat, porcine, mouse, and bovine. Their size and spherical shape makes them highly suitable for various patch-clamp measurements, *e.g.* current- and voltage-clamp; a seminal amount of work has regarding identification and characterization of different ion channels has been done at chromaffin cells. Furthermore, the compactness of the cells facilitates high-resolution capacitance measurements, which allows changes in membrane area to be tracked during studies of both exo- and endocytosis. The LDCVs contain a high concentration of catecholamines (around 0.5 M)<sup>43</sup>, allowing high-temporal measurements of the exocytotic release events to be monitored by *single cell amperometry* (SCA) experiments. Chromaffin cells are adherent cells, which attach easily to surfaces, *e.g.* glass, by the formation of a large circular footprint. This creates a great opportunity to study the movement of fluorescently labeled vesicles during the whole process of exocytosis, with fluorescent microscopy techniques like *total internal reflection fluorescence* (TIRF) microscopy. In addition, many of the molecular species involved in the stimulus secretion chain of chromaffin cells are the same as those found in neurons. This makes them a highly attractive model system for studies of exocytosis.<sup>44,45</sup>

### 2.1.2 PC12 cells

The PC12 cell line is a clonal cell line of rat adrenal pheochromocytoma cells a type of neuroendocrine tumor cells, established by Greene and Tischler in 1976. In growth medium, these cells are round to elliptically shaped cells, with tendencies to grow together in small clusters. PC12 cells respond to treatment with nerve growth factor (NGF) proteins, by a cessation in cell multiplication and by the production of neuronal-like processes after around 7 days of treatment. The morphology of these process greatly resembles those of primary sympathetic neurons in cultures. The processes can extend up to 1000  $\mu m$  with numerous varicosities and large degree of branching. Also, the processes tend to come together to form bundles or fascicles.<sup>46</sup>

The cell bodies of the PC12 cells contains similar large-dense core vesicles (LDCVs) as those in chromaffin cells, both when cultured with or without NGF. In addition to these LDCVs, NGF-treated PC12 cells also contains small clear vesicles, which are mostly located in the varicosities and at the ends of process outgrowths. They morphologically resemble the splanchnic terminals innervating the adrenal medulla.<sup>47</sup>

The PC12 cells express all the enzymes involved in catecholamine synthesis except the enzyme phenyl ethanolamine *N*-methyltransferase (PNMT), responsible for the conversion of norepinephrine to epinephrine. Therefore, epinephrine is not produced in PC12 cells, instead dopamine is the predominantly catecholamine species followed by norepinephrine. The catecholamines are loaded and secreted from LDCVs, as observed from chromaffin cells, but in smaller amounts. LDCVs in PC12 cells contains roughly 0.1 M of catecholamines compared to 0.5 M in chromaffin vesicles.<sup>47</sup>

The fact that PC12 cells are capable of stimulated secretion of electroactive catecholamines and can be differentiated (NGF-treatment) to a neuronal-like cell, makes them a highly attractive model system for exocytosis in neuronal and endocrine systems.<sup>48</sup>

## 2.2 Exocytosis and the SNARE-Machinery

The process of exocytosis is a ubiquitous cellular process that involves the merging of two phospholipid-bilayer membranes to create a fused state. This fused state is instrumental in intercellular communication; since it facilitates the release of neurotransmitters and/or hormones that can propagate an electrical signal between cells by the means of a chemical mediating signal. In order to merge two phospholipid-bilayers, ionic repulsive forces have to be overcome.<sup>49</sup> The force to do this is delivered in highly synchronous fashion by a group of proteins called the SNARE's, the acronym for *soluble NSF Attachment Protein Receptor*, where *NSF* stands for *N-ethylmaleimide sensitive factor*. A simplified diagram of the SNARE complex in vesicle fusion. The SNARE protein family contains over 30 members and each is localized to distinct subcellular compartments. A common structural feature of all SNARE proteins is a 60-70 amino acid long domain, referred to as the SNARE motif.<sup>50</sup> During exocytosis, three related proteins *synaptobrevin* (*syb*) also known as *vesicle associated membrane protein* (VAMP), *syntaxin* (*stx*), and *synaptosomal-associated protein* (25 kDa) (SNAP-25) assemble into a functional complex referred to as the core complex shown in Figure 4. The core complex is the minimum release-capable structure that organizes into a rod-like coiled-coil structure of the four  $\alpha$ -helices.<sup>51</sup> Vesicle fusion with the plasma membrane is induced by the influx of  $Ca^{++}$ , which triggers the full zipping of the coiled complex, and delivers enough force to overcome the repulsive interactions between the membranes.<sup>52</sup>

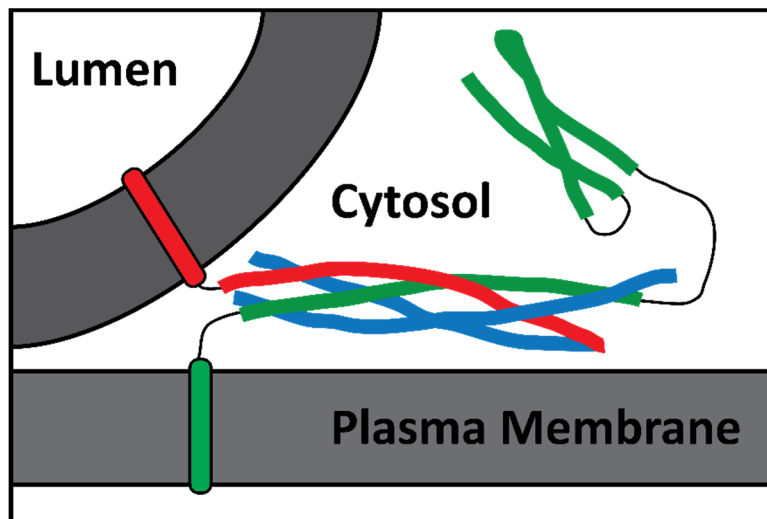


**Figure 4** A cartoon showing the structure of the resembled SNARE core complex, with *synaptobrevin* in **RED**, *syntaxin* in **Green**, and the two SNAP-25 motifs in **Blue**. Adapted from ref 51.

The importance of the SNARE proteins in the exocytotic process is illustrated by the fact that in their absence fusion events are rarely seen, as shown by the action of *Botulinum toxin* (Botox) and various knock-out models. The machinery for vesicular release employs many different molecular players, in particular the SNARE proteins (as described above) but also the *sec1/Munc18-like* (SM) proteins and *NSF* as well as other associated proteins like *complexin* and *synaptotagmin*. The later stages of exocytosis are commonly divided into four distinct stages. These are 1; the *transport* and *docking* of the vesicle to the plasma membrane, 2; several *priming* events, 3; an increase in the releasability of the vesicle and 4; fusion triggered by elevated intracellular  $Ca^{++}$  levels.<sup>52</sup>

## 2.3 Secretory Vesicles

A chromaffin cell contains a vast number of secretory vesicles, approximately 20,000 large-dense core vesicles (LDCVs) making up for roughly 30% of the total cellular volume.<sup>53</sup> The LDCV contains an astonishing high concentration of catecholamines (CA), in the range of 0.5 to 1 M together with 120 to 200 mM of ATP.<sup>54-56</sup> It has been observed that the ratio of ATP:CA has a fixed ratio of about 1:4.<sup>56,57</sup> The vesicles also contain around 15 mM of ascorbate, approximately 40 mM of bound  $\text{Ca}^{++}$ , and 50 to 100  $\mu\text{M}$  of free  $\text{Ca}^{++}$ .<sup>56-59</sup> The high concentration of vesicular solutes provides a theoretical osmolarity of 1500 *mOsm* compared to 315 *mOsm* in the cytosol, which would create a huge osmotic pressure if not accounted for.<sup>60,61</sup> The osmotic pressure can be reduced by aggregation resulting in a decrease in the apparent concentration of the solutes inside the vesicle.<sup>62,63</sup> In fact, the majority (>99%) of the intra-vesicular  $\text{Ca}^{++}$  is found in its bound form interacting with a group of proteins called the chromogranins. The chromogranins (Cg) A, B and C (secretogranin II) are soluble acidic proteins that constitutes the major proteinic content of the vesicles (>80%). They are capable binding  $\text{Ca}^{++}$ , CA and ATP with low affinity but high capacity.<sup>64</sup> The chromogranins is accounted for almost all  $\text{Ca}^{++}$  binding (>99%), but knock-out models of CgA and CgB suggests that the chromogranins are only responsible for around 20% of the CA binding.<sup>65</sup> Hence, another mechanism of complexation of CA should exists. Indeed, *in vitro* studies of the interaction between ATP and CA *in vitro* with NMR, ITC and electrochemistry suggest that a weak complex between ATP and CA in a ratio between 1:1 to 1:4 (ATP:CA) can be formed.<sup>67-69</sup> In addition to the chromogranins, the vesicles also contains bioactive peptides like *neuropeptide Y* (NPY) and enkephalins.<sup>70</sup>

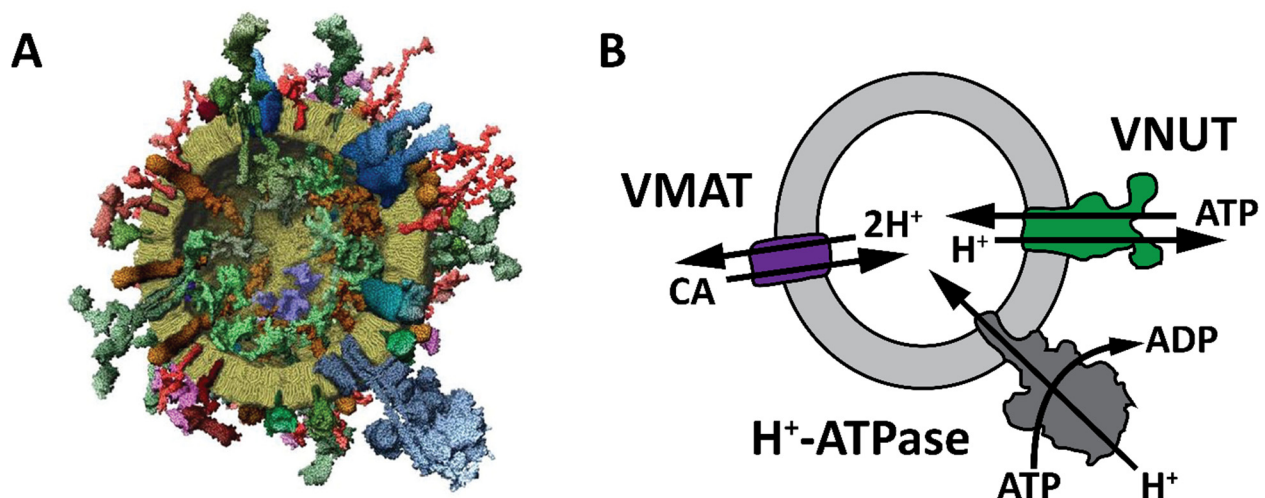


**Figure 5** In (A) a synaptic vesicle is shown scaled to natural proportions and with the estimated amount of proteins, reprinted with permission from Ref 71. In (B) is a schematic of a vesicle with the pumps responsible for loading.

The structure of the vesicle can be represented as a protein decorated liposome (a hollow sphere formed from a single lipid bilayer), see Figure 5. A single vesicle contains a large amount of different membrane bound proteins, and in addition to the previously described proteins like synaptobrevin (syb or VAMP), synaptotagmin (syt) and dopamine- $\beta$ -hydroxylase (DBH);<sup>70</sup> three transporter proteins responsible for the loading spanning the vesicular membrane are present, namely the *vesicular nucleotide transporter* (VNUT), the *vesicular monoamine transporter* (VMAT) and a *vacuolar-type H<sup>+</sup>-ATPase* called V-ATPase. The V-ATPase harvests energy from the hydrolysis of ATP to ADP in order to pump protons against an electrochemical gradient into the vesicles. As a result, the pH inside of the granules is around 5.5, which is two orders of magnitude higher in concentration of H<sup>+</sup> than in the cytosol, which has a pH of 7.4.<sup>72</sup> The low pH has two important biological implications; the first is that chromogranins are acidic proteins with maximum stability and binding capacity around pH 5 (due to the pI of chromogranins in the range of 4.6 to 5).<sup>73</sup> The second, is the other two transporter proteins VNUT and VMAT also utilize the H<sup>+</sup> gradient across the membrane to transport ATP and CA, respectively, into the vesicular lumen (inside). The VNUT pumps in one ATP molecules per proton pumped out, whereas VMAT uses two protons per CA pumped in to the lumen.<sup>74</sup> The transport of CA by VMAT includes three steps, the first involves the binding of H<sup>+</sup> on the luminal side of the transporter that causes a structural change, making the active transport site of CA available at the cytosolic side. Once the CA is bound a second H<sup>+</sup> is required to transport the CA to the luminal side and release the two protons out to the cytosol.<sup>75,76</sup>

As mentioned initially, chromaffin vesicles belong to a group of secretory organelles called large-dense core vesicles (LDCVs). The term *dense-core* stems from the appearance of the aggregated chromogranins in transmission electron micrographs. The protein core is strongly stained by heavy metals, such osmium, uranium or lead during the sample preparation that results in an opaque black spot in the micrograph, due to the low transmission of electron in this region. The *dense-core* is often surrounded by a clear white region, commonly referred to as the *halo*. The size of the *halo* can increase and decrease pharmacologically by the treatment of L-DOPA and reserpine, respectively.<sup>77</sup> The terminology *halo* and *dense-core* is commonly used to distinguish between two distributions of CA inside the granules, the bound (*dense-core*) and the free (*halo*).<sup>78</sup>

## 2.4 Regulatory Mechanisms

The activity of exocytosis can generally be divided into three main modes, namely the *full-fusion*, *kiss-and-run* modes, and more recently the idea of partial release in a more full exocytosis fashion with the vesicle opening and closing again to produce release previously thought to be full release, and yet closing again as with kiss-and-run release. During, *full-fusion* events the secretory vesicle fully collapses and merge with the plasma membrane of the cells; and consequently, the full content of the granule is released into the extracellular space.<sup>79</sup> This mode of exocytosis was for a long time thought to be the only mode of release, however, during patch-clamp recordings of exocytosis in the mid 90's, transient capacitance steps could be observed. These capacitance steps were attributed to granules fusing with the membrane by the formation of a so-called fusion pore, which subsequently closed to recapture the vesicles fully morphological intact.<sup>80</sup> The soluble low molecular weight content (*e.g. catecholamines*) that was released through the transient fusion pore could be observed in amperometric recordings. These new observations led to the postulation of a second mode of release called *kiss-and-run* exocytosis.<sup>81,82</sup> A common feature of the exocytotic spike, regardless of the release mode, is the *pre-spike foot/feature* (PSF), which is the formation of a narrow fusion pore (0.5 to 3 nm in diameter). The PSF is observed as a stable plateau in amperometric recordings, preceding the main spike that is the expansion and closing of the fusion pore. In the last 10 years a variation of release between the classic *kiss-and-run* mode and full release have been reported.<sup>79,83,84,85</sup> This mode has been called *extended kiss-and-run*, *open-and-closed*, or *partial full release* and involves the re-formation of the narrow fusion pore structure after the main event. When a transient release is observed at this stage, it is called a *post-spike foot* because it is similar to the PSF.<sup>84</sup> This partial release mode is thought to be the dominant release mode in model systems studied to date.<sup>79</sup> Another variation in release, is the *flickering* mode that is the repetitive opening and closing and/or fast oscillation in the size of the fusion pore that can be observed as a rapid fluctuation in measured currents or capacitance in amperometric and capacitance measurements, respectively.<sup>86-88</sup> Simultaneous to the experimental results showing partial release, in 2010, Amatore *et. al.* evaluated in a theoretical study the maximum aperture necessary for a complete expulsion of the catecholamine from large dense-core vesicle. They found that the vesicle only had to open about 10 degrees (corresponding to a  $\varnothing$ 17 nm pore for a  $\varnothing$ 200 nm vesicle) for the observation that was thought to be full catecholamine release from a vesicle and concluded that most cases of exocytotic release observed by amperometry were in fact partial.<sup>85</sup> At these small opening angles, the major part of the dense-core matrix is still surrounded by membrane so release cannot be full. The combination of experimental and

theoretical results led to the need for new terminology and the invention of *partial* and *full release*, which is not referring to the faith of the granules (even though the *kiss-and-run* mode is often assumed) instead the faith of the content.<sup>79</sup>

One of the major factors controlling the modes of release and consequently the amount released, is the strength of the stimuli used to induce *exocytosis*. This has been illustrated in studies using *artificial action potentials* (AAPs) to electrically evoke secretion events. Here it has been shown that if the frequency of AAP trains is increased from 0.25 Hz to 10 Hz in a 2 mM  $[Ca^{++}]_o$  (extracellular  $Ca^{++}$  concentration) or altering  $[Ca^{++}]_o$  from 0.25 to 7 mM at a fixed stimulation frequency of 7 Hz the same gradual increase in amount released (quantal size) is observed.<sup>89</sup> This was further confirmed by Fulop *et. al.* in a study where they matched low frequency (0.5 Hz) AAP stimulation to 10 mM  $K^+$  stimulation and high frequency (15 Hz) to 30 mM  $K^+$ . They observed that the intracellular  $Ca^{++}$  levels increased with elevated strength of the stimuli followed by a dramatic increase in the amount release.<sup>89-91</sup> These observations highlight the importance of intracellular  $Ca^{++}$  levels not only for initiation of exocytosis but also its regulation. Elevated intracellular  $Ca^{++}$  levels have been shown to significantly increase the reorganization of F-actin (*filamentous actin*), a major component of the cytoskeleton. The F-actin network is present at the highest density close the *plasma membrane* and acts as the major force on the membrane responsible for shaping the cell. Consequently, *F-actin* also acts as a physical barrier that must be reorganized in order for vesicles to be transported to the sites of release. Several studies, using potent *actin*-polymerization blockers such as, cytochalasin D and latrunculin A, have been shown to not only increase the frequency of exocytosis release events, but also to increase the number of molecules released per event.<sup>90,92</sup> The opposite effect, a reduced release frequency and a decrease in the amount release, was observed as an effect of incubation with jasplakinolide, a stabilizer of F-actin.<sup>90</sup> These observations strengthen the hypothesis that the actin cytoskeleton acts as a closing force constraining the opening and expansion of the fusion pore during exocytosis.

Intracellular  $\text{Ca}^{++}$  ion also acts as *secondary messenger* capable of activating *protein kinase C* (PKC) by binding to its  $\text{C}_2$  domain. PKC in its activated form is capable of rapid phosphorylation of the protein Munc18-1, which alters its affinity to the SNARE core-complex protein syntaxin. Phosphorylation of Munc18-1 reduces the affinity to bind the SNARE core-complex and allows it to dissociate and leave the SNARE core-complex in a primed configuration. By creating mutants of Munc18-1 that could not be phosphorylated by PKC the number of release events was significantly reduced by locking the SNARE core-complex in an unprimed state.<sup>93</sup> This was also demonstrated in another study by Voets *et. al.*, where they acutely overexpressed Munc18-1 in bovine chromaffin cells. The overexpression of Munc18-1 reduced the frequency of events to 10% of control, but did not alter the kinetics of the remaining release events.<sup>94</sup>

Myosin II is an ATP-dependent motor protein that recruits vesicles to the readily releasable pool in chromaffin cells and is known to interact with *actin*. The activity of myosin II is regulated by the phosphorylation of the *myosin light chain kinase* (MLCK), which is dependent on  $\text{Ca}^{++}$  ion and *calmodulin* (CaM). It was found by expressing a phosphorylation incompetent form of myosin II *regulatory light chain* (RLC) that the dynamics of *catecholamine* release was reduced, as well as the amount released.<sup>90,95</sup> In similarity to the PKC pathway and in coherence with the seemingly important regulatory mechanism of phosphorylation during exocytosis, the *protein kinase A* (PKA) pathway can also significantly alter the modes of release. This was demonstrated in a study by Machado *et. al.* who looked at the effect of cholera toxin and the drug forskolin on exocytosis; both cholera toxin and forskolin are known to raise the intracellular levels of *cyclic adenosine monophosphate* (cAMP), a *secondary messenger* that activates PKA. They found that elevated levels of cAMP modulated the last steps of exocytosis, and the effect of both cholera toxin and forskolin could be attenuated by the addition of the PKA inhibitor H-89.<sup>96</sup>

The process of exocytosis requires the merging of two membranes (the vesicular and plasma membrane) to establish a pore through which some or all of the vesicular cargo can be released. This has led to the hypothesis that incubation of different lipids could potentially alter the stability and formation of the fusion pore. This was tested in a study by Uchiyama *et. al.* where they incubated PC12 cells with *phosphatidylcholine* (PC), *phosphatidylethanolamine* (PE), *phosphatidylserine* (PS), *sphingomyelin* (SM), and *phosphatidylinositol* (PI). They found that PC significantly reduced the amplitude and the amount released, while electron micrographs showed a 50% increase in the size of the vesicles. In contrast to PC, PE increased the release rate with larger amplitude and reduced time course compared to control, but no significant difference in the amount released was observed. The incubation with PS increased the number of observed events by 1.7-fold, which was attributed to increased recruitment of vesicles estimated from

analysis of the electron micrographs. In addition to the increased release frequency, the overall time course of the release event was significantly slower, indicating a reduction in the rate of fusion pore expansion. However, the addition of PI did not cause any significant changes in the amperometric response.<sup>97</sup> In another study, incubation of cholesterol has been demonstrated to increase both the rise time and fall time, as well as, increase the fraction of pre-spike foot (PSF) events from 30% to 50%, and to prolong the average duration of these PSF's.<sup>98</sup> These observations are consistent with the observation that cholesterol promotes the formation of negative curvature structures *in vitro*, which provides a plausible explanation for the apparent increase in the fusion pore stability.<sup>99,100</sup> Cholesterol has also been shown to be crucial for the formation of syntaxin (a protein member of the *SNARE core-complex*) clusters in the plasma membrane. Depletion of cholesterol from the membrane by the addition of cyclodextrin significantly reduced the frequency of exocytosis, but without any significant changes in the kinetics of the observed release events.<sup>101,102</sup> This suggests that cholesterol might have a role in the creation of the micro-environment necessary for proper function of the SNARE-machinery, in addition to the pure membrane mechanistic aspects described previously. Other agents capable of perturbation of the plasma membrane are *sodium dodecyl sulfate* (SDS) and *dimethyl sulfoxide* (DMSO, **paper VII**). Both significantly increase the amount released per event.<sup>103,104</sup> Incubation of cells with 0.6% DMSO for 30 min increased the fraction released from 53% to 92%, as measured by *intracellular impact electrochemical cytometry* (IVIEC) and *single cell amperometry* (SCA). DMSO also increased the life-time of the PSF by 50%. These observations were suggested to be a result of reduced membrane tension resulting from introduction of water pores in the membranes and a concurrent reduction in membrane thickness.<sup>105</sup> It was also speculated that DMSO can readily cross the plasma membrane and interact with proteins of the SNARE-machinery or dynamin, which have all been shown capable of generating similar effects.<sup>105</sup>

---

## 3 Electrochemical Theory

---

In this section, the theory behind electrochemical reactions and systems will be addressed. The convention in this thesis is that oxidation current (anodic) is shown as positive and reduction (cathodic) is shown as negative. Further, positive potential is presented on the right and negative is presented on left in voltammograms, and all reactions will be considered as one electron transfer reactions.

### 3.1 General Electrochemical Kinetics

If the single step reaction described in Eq. 3. is considered, a reduced (*Red*) species is oxidized into its oxidized form (*Ox*) leaving  $n$  number of electrons ( $n$  is an integer, usually 1 or 2) during the process.



Both reactions are active at all times, the rate of the oxidation and reduction process can be described as following,

$$v_{Ox} = k_A C_{Red} \quad \text{Eq. 4}$$

$$v_{Red} = k_C C_{Ox} \quad \text{Eq. 5}$$

where  $k_A$  and  $k_C$  are the rate constants of the oxidation and reduction process with the unit  $s^{-1}$ , and  $C_{Red}$  and  $C_{Ox}$  is the concentration of the reduced and oxidized species respectively. The net conversion rate,  $U_{net}$ , can be written as follows.

$$v_{net} = v_{Ox} - v_{Red} \quad \text{Eq. 6}$$

At equilibrium, the net conversion rate is zero, which yields the following expression for the equilibrium constant  $K$ ,

$$K = \frac{k_A}{k_C} = \frac{C_{Ox}}{C_{Red}} \quad \text{Eq. 7}$$

The reaction rates can also be described in terms of currents, where the current ( $i$ ) is the product of rate constant ( $k$ ) and the surface concentration  $C(0,t)$ . As the electrode only can respond to its

immediate surroundings the concentration for the expression  $C(0,t)$  is the concentration at the electrode surface at time  $t$ , which allows us to write an expression for the conversion rate for the oxidation (anodic) process as,

$$v_{Ox} = k_A C_{Red}(0, t) = \frac{i_A}{nFA} \quad \text{Eq. 8}$$

whereas the rate of conversion for the reduction is described as

$$v_{Red} = k_C C_{Ox}(0, t) = \frac{i_C}{nFA} \quad \text{Eq. 9}$$

Here,  $F$  is the *Faraday constant* that defines the charge of one mole of electrons and  $A$  is the surface area of the electrode in  $cm^2$ .

Since we now have a way to relate surface concentration and rate constants to current, we can write an expression for the net current ( $i_{net}$ ) through the system based on the anodic ( $i_A$ ) and cathodic current ( $i_C$ ) component, hence,

$$i = i_A - i_C = nFA[k_A C_{Red}(0, t) - k_C C_{Ox}(0, t)] \quad \text{Eq. 10}$$

The rate constant  $k$  can further be described in terms of *standard free energy of activation* ( $\Delta G^\ddagger$ ) by the *Arrhenius equation*, as follows,

$$k = A e^{-\Delta G^\ddagger/RT} \quad \text{Eq. 11}$$

where  $A$  is the frequency factor,  $R$  is the general gas constant and  $T$  is the temperature in Kelvin. The concept of activation energy can be used to illustrate the reaction path in terms of potential energy along a reaction coordinate as shown in Figure 6.

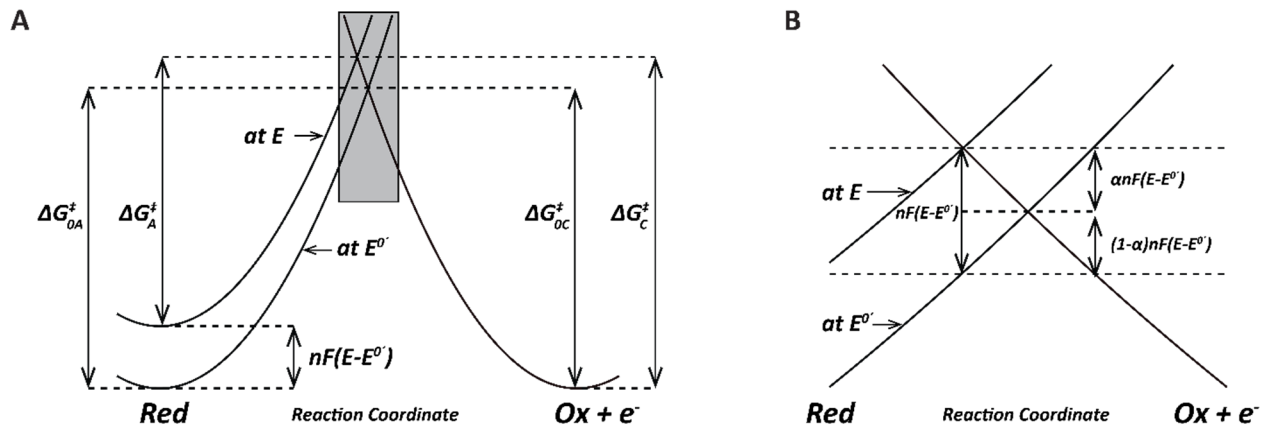


**Figure 6** In (A) is the effect of a potential changes on the standard free energies of activation energy for oxidation and reduction and (B) relationship of the transfer coefficient to the angles of intersection of the free energy curves.

$E^0$  is the potential at equilibrium, commonly referred to as *the formal redox potential*, where the potentials  $\Delta G_{0A}^\ddagger$  and  $\Delta G_{0C}^\ddagger$  have the same magnitude. Consequently, the anodic and cathodic process has the same activation energy, in other words both processes have the same rate constant. The excess of polarization from *the formal redox potential* ( $E^0$ ) is measured by the *overpotential* ( $\eta$ ), that is

$$\eta = E - E^0 \quad \text{Eq. 12}$$

When the potential at the electrode is increased, the activation energy barrier for the anodic process  $\Delta G_A^\ddagger$  is decreased, meanwhile the activation energy barrier for the cathodic  $\Delta G_C^\ddagger$  is increased. Now the anodic process runs faster than the cathodic, leading to a shift from the reduced to the oxidized form. In Figure 6, a reversible system is described, commonly referred to as a *Nernstian* system. In such systems, the *transfer coefficient*,  $\alpha$ , is typically taken as 0.5, which has the implication that the system is symmetric in regard to the activation energy barrier for the reactions. The change in the activation energy barrier for the corresponding anodic and cathodic process as can be written as,

$$\Delta G_A^\ddagger = \Delta G_{0A}^\ddagger - (1 - \alpha)nF\eta \quad \text{Eq. 13}$$

$$\Delta G_C^\ddagger = \Delta G_{0C}^\ddagger + \alpha nF\eta \quad \text{Eq. 14}$$

By the insertion of the expression for the activation energies (Eq. 13 and 14) into the *Arrhenius equation* (Eq. 12), the following expressions are obtained

$$k_A = A_A e^{(-\Delta G_{0A}^\ddagger/RT)} e^{[(1-\alpha)f\eta]} \quad \text{Eq. 15}$$

$$k_C = A_C e^{(-\Delta G_{0C}^\ddagger/RT)} e^{[-\alpha f\eta]} \quad \text{Eq. 16}$$

where  $f = nF/RT$ . The first factor in both Eq. 15 and 15 describes the rate at equilibrium ( $E^0$ ). This value is called the *standard rate constant* ( $k^0$ ). Thus, the rate constant at other potentials can be described in terms of  $k^0$  by following expression.

$$k_A = k^0 e^{(1-\alpha)f\eta} \quad \text{Eq. 17}$$

$$k_C = k^0 e^{-\alpha f\eta} \quad \text{Eq. 18}$$

Taking these new expressions for the rate constants of the anodic and cathodic process and inserting them into Eq. 10, following expression is obtained

$$\boxed{i = nFAk^0 [C_{Red}(0, t)e^{(1-\alpha)f\eta} - C_{Ox}(0, t)e^{-\alpha f\eta}]} \quad Eq. 19$$

which is commonly referred to as the *Butler-Volmer equation*. This formulation has proven very useful for dealing with almost any heterogeneous reaction.

If we now consider the special case where the net current ( $i$ ) is zero, consequently  $i_A$  is equal to  $i_C$  and we get following expression.

$$nFAk^0 C_{Ox}(0, t)e^{-\alpha f\eta} = FAk^0 C_{Red}(0, t)e^{(1-\alpha)f\eta} \quad Eq. 20$$

Again, we have an expression describing the equilibrium, where the anodic and cathodic processes have the same rates. Simplifying Eq. 21, yields,

$$e^{f\eta} = \frac{C_{Ox}(0, t)}{C_{Red}(0, t)} \quad Eq. 21$$

which is just the logarithmic form of the *Nernst equation* (Eq. 22).

$$\boxed{E(t) = E^{0'} + \frac{RT}{nF} \ln \left( \frac{C_{Ox}(0, t)}{C_{Red}(0, t)} \right)} \quad Eq. 22$$

Since  $\eta$  is equal to  $(E - E^{0'})$ , this tells us that when  $E = E^{0'}$ . The surface concentrations of the oxidized and reduced forms are equal, that is  $C_{Ox}(0, t) = C_{Red}(0, t)$ . I will return to this later when introducing the *general wave equation* during the discussion of steady-state cyclic voltammetry.<sup>106</sup>

## 3.2 Chronoamperometry

Chronoamperometry is a potential step method, where the potential is switched from a potential  $E_1$  to a potential  $E_2$ . If the analyte of interest is initially in its reduced form, the potential  $E_1$  is usually negative with respect to the formal redox potential and  $E_2$  is positive. Consequently, at the forward step  $E_1$  to  $E_2$  shown in Figure 7A the anodic process is dominant (*oxidation*) and at the reverse the cathodic process (reduction) dominates. This gives a characteristic  $i$ - $t$  curve shown in Figure. 7B.

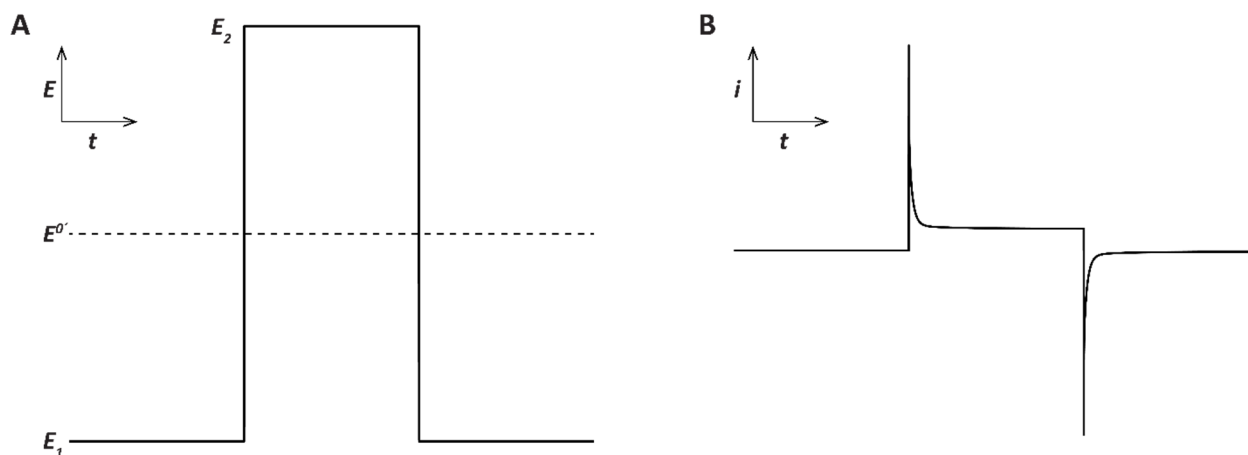


**Figure 7** Shown in (A) is the waveform for chronoamperometry where the potential is step back and forth between the potentials  $E_1$  and  $E_2$ , resulting a square-wave shaped waveform. In (B) a current response to the changed potentials is shown, a sharp spike decaying towards *steady-state* due to the *consumption/conversion* of electroactive species at the electrode surface, as well as a rapid charging and discharging of the electrical double-layer (background).

The potential switching initially induces a large current due to the onset of the *faradaic* process (a *redox* reaction) and an RC component (background) due to the charging of the electrode surface. However, the background decays relatively rapidly as an exponential function vs. time with a time constant  $\tau = R_s C_d$ , where  $R_s$  is the series of resistances in the circuit and  $C_d$  is the capacitance of the double-layer. As a result, during a period of approximately three time-constants, the contribution from the charging current substantially influences the total current measured (contribution > 5%), which makes it difficult to determine the *faradaic* current accurately. However, after this period the faradaic process dominates the observed current. As the analyte is *consumed* (converted) a concentration gradient is created from the electrode surface to the bulk solution, this is called the depletion layer.

The expansion of the depletion layer causes a time dependent decline in the measured *faradaic current* due to reduced mass-transport towards the electrode surface; the measured current for electrolysis at a disk electrode during this behavior can be described by the *Cottrell equation* as,

$$i(t) = \frac{nF\sqrt{D\pi}C^*r^2}{\sqrt{t}} \quad \text{Eq. 23}$$

where  $i(t)$  is the current as a function of time,  $n$  is the number of electrons transferred during the reaction,  $F$  is the Faraday constant,  $C^*$  is the bulk concentration of the analyte of interest,  $r$  is the radius of the electrode and  $D$  is the diffusion coefficient. By fitting experimental data to the equation additional information about the system can be acquired, such as diffusion coefficient, concentration or effective radius of the electrode.

The *Cottrell equation* cannot be used to describe the time dependency of the current at micro disk electrodes, due to the heterogenous nature of the diffusion profile at those electrodes. As shown before, the diffusion profile at macro electrodes is dominated by linear (one-dimensional) diffusion and for micro disk electrodes the mass-transport is dominated by spherical (two-dimensional) diffusion. Consequently, the current density at a microelectrode is larger at the edges, the so-called *edge effect*. Aoki and Osteryoung were the first to report a theory including *the edge effect* in 1981, which was refined by Shoup and Szabo one year later to give an empirical solution better than 0.6% for all times, the result is referred to as *the Shoup-Szabo equation*.<sup>107-109</sup>

$$i(t) = 4nFDC^*rf(t) \quad \text{Eq. 24}$$

$$f(t) = 0.7854 + 0.8862\sqrt{\tau} + 0.2146e^{(-0.7823\sqrt{\tau})} \quad \text{Eq. 25}$$

$$\tau = \frac{r^2}{4Dt} \quad \text{Eq. 26}$$

$$i_{ss} = 4nFDC^*r \quad \text{Eq. 27}$$

Here, all components are the same as in the *Cottrell equation*. The function in *Eq. 25* describes the expansion of the depletion layer as a function of time and decays towards 1 at a rate dependent on the electrode radius,  $r$ , and the diffusion coefficient,  $D$ , according to *Eq. 26*. It is worth noticing that *Eq. 27* is the same as *the Shoup-Szabo equation (Eq. 24)* at large  $t$ 's (steady-state) as a result of the function in *Eq. 25* being equal to 1 at these times. For a micro disk electrode with a radius of  $2.5 \mu\text{m}$  in solution of dopamine ( $D = 6 \times 10^{-6} \text{ cm}^2\text{s}^{-1}$ ) the measured current is less than 5% from steady-state after 0.5 s. This fast equilibration allows information to be retrieved both from the steady-state and the non-steady-state regimes in a single

measurement. Since, *Eq. 27* is used for the steady-state regime and *Eq. 24* for the non-steady-state regime, information about  $r$  or  $D$  can be retrieved simultaneously with information about  $n$  or  $C$ . This is only true for microelectrodes, but the same information can also be obtained at macroelectrodes by for example using rotating disk electrode (RME) experiments. These experiments are not described here.<sup>106</sup>

### 3.3 Cyclic Voltammetry

Cyclic voltammetry (CV) is a potential sweep method where the potential is continuously changed from a potential,  $E_1$ , to a potential,  $E_2$ , and then back again to  $E_1$ , resulting in a triangular waveform as shown in Figure 8B. As in chronoamperometry, the initial potential  $E_1$  is typically in a region of *non-faradaic current* e.g. 200 mV positive or negative of the *formal redox potential*  $E^{0'}$  of the system of interest. When the potential is increased the energy levels of the electrode is also increased leading to an onset of the reaction as the *activation energy barrier* is decreased (see Figure 6). This is shown as sharp increase in the current response as a function of potential both for micro (Figure 8A) and macro (8C) electrodes.

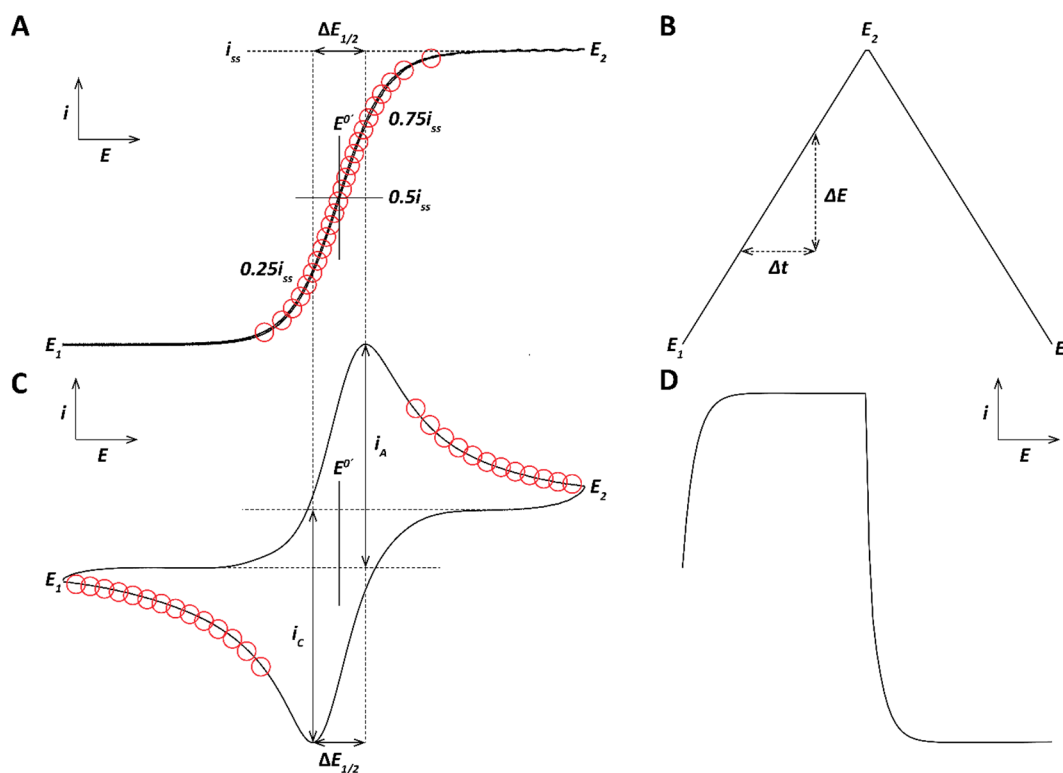


**Figure 8** In (A) a voltammogram from a CFME is presented, showing the sigmoidal *current-potential* relationship during steady-state voltammetry. The red dots in (A) is the theoretical behavior predicted by the *general wave equation*. In (B, inlet) the waveform used for both voltammograms in A and B, obtained by ramping the potential  $E_1$  via  $E_2$  back to  $E_1$  with a scan rate described by  $\Delta E / \Delta t$ . In (D) the response of an ideal capacitor to the applied waveform (B) is shown, which is the background component (not scaled) of the voltammograms (A) and (C).

For microelectrodes, the depletion layer equilibrates faster than the potential increase, and therefore results in a sigmoidal voltammogram reflecting the charge transfer rates as a function of the potential. The relationship between current and potential is described by the *general wave equation* as follows.

$$E(t) = E^{0'} + \frac{RT}{nF} \ln \left( \frac{i(t)}{i_{ss} - i(t)} \right) \quad \text{Eq. 28}$$

This is derived from the *Nernst equation*, by expressing the surface concentration of the oxidized ( $C_{Ox}(0, t)$ ) and reduced ( $C_{Red}(0, t)$ ) species in terms of currents. The term  $i_{ss}$  is the current at steady-state previously described in Eq. 27 of the Chronoamperometry section, and  $i(t)$  is the measured current at the time  $t$ . The current  $i(t)$  and the potential  $E(t)$  is related through the scan rate ( $v = \Delta E / \Delta t$ ). The potential  $E(t)$  is equal to the *formal redox potential* ( $E^{0'}$ ) when the current  $i(t)$  is half of the current at steady-state ( $0.5 i_{ss}$ ). At this potential, the surface concentration of the oxidized and reduces species is equal and, under *Nernstian conditions*, the rate of oxidation is equal to the rate of reduction. The reversibility can be evaluated for microelectrodes by the *Tomeš criterion*,

$$\Delta E_{1/2} = E_{3/4} - E_{1/4} = E_{i_A} - E_{i_C} = \frac{RT}{nF} 2.197 = 56.4 \text{ mV}/n \quad \text{Eq. 29}$$

where  $\Delta E_{1/2}$  is the difference between the potential  $E_{3/4}$  and  $E_{1/4}$ , which is the potential at 75% and 25% of the steady-state current, respectively. This is equivalent to the difference in potential between the anodic ( $i_A$ ) and cathodic ( $i_C$ ) peaks for macro electrodes, which is equal to 56.4 mV/ $n$  at 25° Celsius (298K) for *Nernstian systems* (see Figure 8A and C).<sup>106</sup>

Furthermore, the magnitude of the peak current for a *Nernstian system* is described by the *Randles-Ševčík equation* for various electrode geometries as shown in Table 1,

**Table 1.** Table of geometry specific functions and constants for *Randles-Ševčík equation*.<sup>111</sup>

Geometry	$\Psi(p)$
Inlaid disk (macro)	0.446
Spherical/hemispherical	$0.446 + 4/\pi p^{-1}$
Cylindrical/hemicylindral	$0.446 + 3.44p^{-0.852}$

The *Randles-Ševčík* equation is given as,

$$i_{lim} = -\Psi(p) \left( \frac{n^3 F^3 \nu D}{RT} \right)^{1/2} AC \quad \text{Eq. 30}$$

$$p = \left( \frac{nF\nu}{RT} \right)^{1/2} \quad \text{Eq. 31}$$

where,  $\nu$  is the scan rate, and all the other variables are as described above. The parameter  $\Psi$  takes the electrode geometry into account, for planar disk macro electrodes  $\Psi$  is equal to 0.446 and the peak current is proportional to the square root of the scan rate. For a microelectrode (see spherical and cylindrical),  $\Psi$  considers the increased current due to the *edge-effect* described earlier in the chronoamperometry section. Additionally, the parameter  $p \ll 1$  leading to steady-state conditions prevails (current is diffusion limited), if either the scan rate or the radius increases such that  $p \gg 1$ , *macro* behavior is observed due to a time dependent depletion effect, non-steady state conditions.<sup>110,111</sup>

By sweeping the potential, the double layer (background) is constantly charging and discharging, however, in CV the resistive component  $R_s$  in the expression  $R_s C_d$  can be neglected. Consequently, the charging current in CV can be described as a pure capacitor with a constant potential response as shown in Figure 8D. The magnitude of the charging current is directly proportional to the scan rate ( $\nu$ ) and the peak currents ( $i_A$  and  $i_C$ ) are only proportional to the *square-root* of the scan rate.

### 3.4 Connecting Chronoamperometry and Cyclic Voltammetry

To summarize, chronoamperometry and cyclic voltammetry are to a large degree connected by the common parameter of time. In Figure 9A, three simulated voltammograms at different scan rates for a microelectrode are shown; the first (orange) voltammogram, has the largest scan rate and the full cycle from  $E_1$  to  $E_2$  and back to  $E_1$  takes the shortest time to complete. At these fast scan rates, depletion effects are observed due to a rapid increase in the applied potential, and the response can partially be described by the *Shoup-Szabo equation* as shown in Figure 9C.

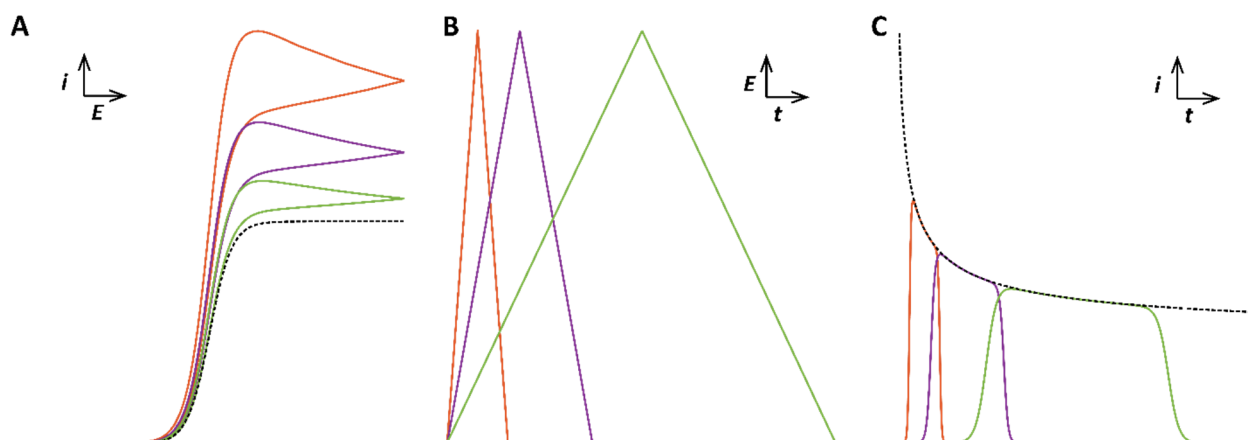


**Figure 9** In (A) three voltammograms are shown, **Orange, Purple** and **Green**. The **Black dotted line** is the steady-state behavior predicted by the *general wave equation*. In (B) are the waveform for the voltammograms in (A) shown, illustrating the different time-courses due to the different scan-rates. In (C) are the current response of the voltammograms in (A) shown as a function of time, illustrating the effect of the expansion of the depletion-layer. The **Black dotted line** in (C) is the  $i-t$  response predicted by the *Shoup-Szabo equation*.

Depending on the scan rate, the current response from the cyclic voltammogram will intercept with the  $i-t$  response at different times. It becomes obvious also that the peak current is proportional to the square-root of the scan rate, hence,  $\sqrt{v}$  is equal to  $\sqrt{\Delta E/\Delta t}$ , and the current  $i(t)$  is proportional to  $\sqrt{1/t}$ . As described previously, if the mass-transport to electrode area is high (e.g. the electrode is small) the scan rate must be large to observe depletion effects. For steady-state voltammetry as in Figure 9A (dotted line) the time to ramp the potential is relatively long, such that the observed current is limited by the mass transport, as described by Eq. 27 and the  $i_{ss}$  term in Eq. 28 (the *general wave equation*).<sup>106,111</sup>



---

## 4 Methods to Study Exocytosis

---

### 4.1 Background of Electrochemistry at Carbon Electrodes

Much of modern electrochemistry was to a large degree pioneered by the work of Ralph N. Adams from the late 1950's up to the mid 80's. In 1958, he published the first paper on carbon paste electrodes, a new type of solid electrode that was produced by mixing graphite powder with a mineral oil like Nujol or organic solvents like bromoform or bromonaphthalene.<sup>112</sup> His research interests until 1969 were mostly focused on electrochemical oxidation pathways of aromatic amines and hydrocarbons.<sup>116,114</sup> In 1967, he reported a study on the electro-oxidation pathways of catecholamines at carbon paste electrodes, which also was included in a review in 1969 proposing the use of electrochemistry in the field of pharmacy and medicine.<sup>115,116</sup> His research focus then switched from mechanistic studies to more problem-oriented research in the fields of neurochemistry and neuropharmacology. In 1973, he reported the first example of electrochemistry in the brain, by implanting a carbon paste electrode in the brain of a rat they could monitor the concentration fluctuations of ascorbic acid.<sup>117</sup> Up until this point in time the only reported applications of *in vivo* electrochemistry were the recordings of oxygen tension with a miniaturized Clark-type membrane electrode in brain cortex by Bicher *et. al.*, and the recordings of cysteine levels in the blood stream and kidney cortex by Koryta *et. al.*<sup>118-120</sup> The Adams group quickly followed the first publication with an additional of three publications in a series of publication called *Voltammetry in Brain Tissue*, which came out between 1973 and 78.<sup>121-123</sup> The potential of these experiments was quickly understood by others and many groups contributed to further develop the methodology.<sup>124-126</sup>

Almost simultaneously with the first reports on *in vivo* electrochemistry, the first report of carbon fiber electrodes came out 1975 by Jennings and Pearson. They fully understood the potential of carbon fiber as microelectrode material, '*Microelectrodes can be used in titration of small volumes, such as those found in biological cells*', but they reported its use as a pH sensitive electrode potentially used for intracellular recordings, which was a hot-topic at that time.<sup>127-129</sup> The use of carbon fibers for electrochemistry of organic molecules had wait until 1979 when Ponchon *et. al.* published the first paper using electrochemistry with a carbon fiber as the working electrode.<sup>130</sup> They used normal pulse polarography and cyclic voltammetry to characterize the electrochemical behavior of catecholamines and their derivatives *in vitro* using a cylindrical carbon fiber electrode. In the same year, the group of Julian Millar reported on the

fabrication and application of carbon fiber electrodes for extracellular single unit recordings (electrophysiology).<sup>131</sup> In 1980, a considerable effort to characterize the properties of carbon fiber electrodes was made; the Millar group reported a study on the electrical properties and the Wightman group reported the development electrochemical characteristics of disk-shaped carbon fiber microelectrodes.<sup>132,133</sup> Additionally, in same the year the Millar group reported the first example of high-speed (fast-scan) cyclic voltammetry (a full waveform cycle in 15 ms), which was used to study the concentration of serotonin (5-HT) ejected by iontophoresis both in *in vitro* and *in vivo*.<sup>134</sup> Also in the year of 1980, Pujol *et. al.* was able to distinguish the DOPAC signal from the ascorbate background by the use of cylindrical carbon fiber electrodes and differential pulse voltammetry (DPV).<sup>135</sup> By this method they could monitor the influence on the DOPAC signal by pharmacology agents like for example pargyline, reserpine and amphetamine. Additionally, they were the first to report on *in vivo* electrochemistry in 1981, which was a continuation of the study from the year before.<sup>136-138</sup> Electrically stimulated release of a transmitter was presented in 1983 by Ewing *et. al.*; where they used a 10 s long 60 Hz pulse-train in combination with cyclic voltammetry to monitor the changes in dopamine concentration following release with a time resolution of a few seconds.<sup>139</sup>

The number of publications rapidly increased in the coming years, and a significant contribution to the theoretical understanding of these electrodes was published in 1981 by Aoki and Osteryoung, which later was refined in 1982 by Shoup and Szabo (as previously mentioned in the electrochemical chapter).<sup>108,109</sup> By the mid 80's *in vivo* electrochemistry was a fully developed research field, and carbon fiber electrodes were the prime electrode material due to the small size, low cost, commercial availability, high biocompatibility, and excellent electrochemical properties.

### 4.1.1 Single Cell Amperometry

In the year of 1990, the Wightman group began performing voltammetric studies on single adrenal chromaffin cells *in vitro*.<sup>140</sup> They observed rapid fluctuations in peak currents between consecutive scans, which they attributed to single exocytotic release events. It could also be further confirmed that the observed current was due to oxidation of released catecholamines.<sup>141</sup> In 1991, the same group reported on the first example of single cell amperometry; By performing the same type of experiments but keep the applied potential constant, the temporal resolution was significantly increased to clearly resolve single exocytotic release events.<sup>142</sup> A similar study was also reported by Neher's group in 1992.<sup>143</sup>

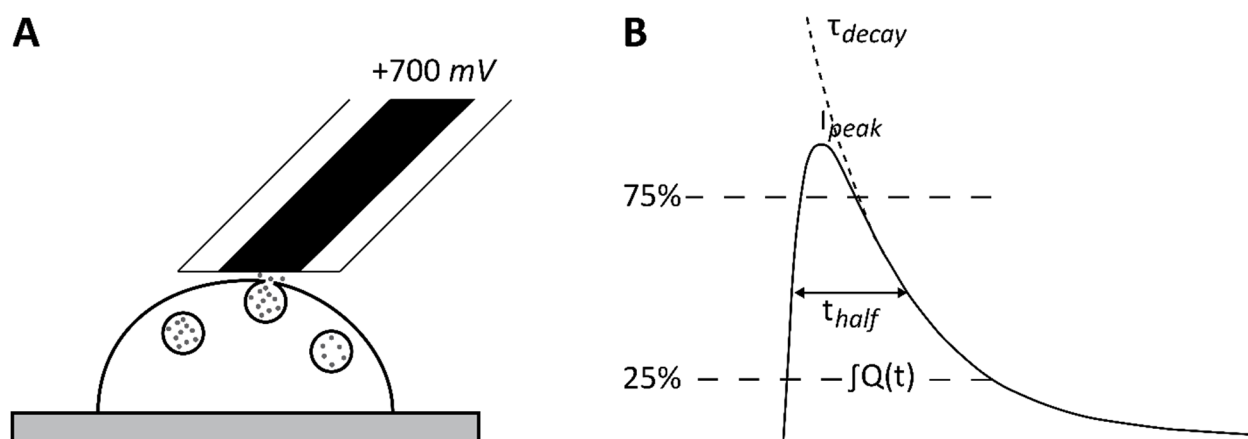


**Figure 10** In (A) a schematic representation of *single cell amperometry* (SCA) with the electrode position at the apex of the cell, the polarized electrode is oxidizing the molecules release and one spike (B) is obtained per release event. The rise time is usually defined as the time span between 25% and 75% of  $I_{max}$ , and the fall time is the opposite. The time duration between 75% and 25% of  $I_{max}$ , and the  $t_{half}$  is defined as the full width at half maximum.

In *single cell amperometry* (SCA), a microelectrode in the size range of a cell ( $\varnothing$  5-10  $\mu\text{m}$ ) is beveled at a 45° angle and positioned on top of a cell in culture. A potential is applied to the electrode and held at sufficient overpotential to guarantee that the observed current is mass transport limited. For studies monitoring the release of catecholamines, a potential of around 700 mV vs. a Ag|AgCl reference electrode is commonly used. In order to trigger release an electrical or chemical stimulus have to be applied in order to increase the intracellular  $\text{Ca}^{2+}$  concentration, which initiate the vesicle fusion. The released molecules reach the electrode surface by means of diffusion and are oxidized immediately. As a result, a current response is observed as a function of time, as shown in Figure 10B. Important information about the release event can be obtained by analyzing the shape of the spike. By integration of individual spikes, the charge (Q) can be obtained;

The charge is directly proportional to the number of moles (molecules) released during the event, as described by *Faraday's law*,

$$N = \frac{Q}{nF} \quad \text{Eq. 32}$$

which can be re-written as,

$$\text{number of molecules} = \frac{Q}{n} K \quad \text{Eq. 33}$$

where  $n$  is the number of electron transferred during reaction,  $F$  is the *Faraday constant*,  $N$  is the number of moles released and  $K$  is equal to *Avogadro's number over Faraday's constant* ( $N_A/F = 6.2415 \times 10^{18}$  *electrons/C*). Additionally, kinetic information about the release event can be obtained from the rise-time ( $T_{Rise}$ ), which reflects the expansion of the fusion pore; and the fall-time ( $T_{Fall}$ ) that represents the closing of the pore and clearance/consumption of release molecules from the extracellular space. The amplitude of the spike ( $I_{Max}$ ) describes the maximum flux (molecules/s or Q/s) and the full width at half maximum ( $T_{1/2}$ ) is an indicator of the overall duration of the event.

### 4.1.2 Vesicle Impact Electrochemical Cytometry

Single cell amperometry is an excellent tool to monitor and quantify the release process at the single cell level, but it is unable to obtain any information about the full vesicular content. Many drugs that affect exocytosis, do so in the earlier stages of the process by affecting the vesicular loading and storage of the cargo. Therefore, it is absolutely necessary to be able to obtain information about full vesicular content to obtain a broader perspective of the release process.

The first report of a method able of quantifying the vesicular content came in 2009 by Omiatek *et. al.* They used capillary electrophoresis and microfluidics in combination with electrochemical detection. The system was setup to separate isolated vesicles by size and charge by capillary electrophoresis, and a sheath flow was created by the microfluidic device to focus vesicles exiting the separation along the axis of cylindrical carbon fiber electrode used for detection. The guiding sheath flow contained a high concentration of sodium dodecyl sulfate (SDS), which caused vesicles to rupture and release their content in close proximity to the detecting electrode.<sup>83,144,145</sup>

In 2015, the Ewing group reported on two new methods capable of vesicular content quantification, namely, vesicle impact electrochemical cytometry (VIEC, **paper II**) and intracellular vesicle impact electrochemical cytometry (IVIEC, **paper III**). These two methods have many similarities, but the procedures to obtain recordings are very different. In VIEC, the vesicles are isolated in the same way as described by Omiatek *et. al.*, but instead of separating the vesicles before detection, the electrode is either *dipped* (incubated) in a concentrated vesicle solution or vesicles are added to the recording solution called *adding*. Both the *dipping* and the *adding* procedures for VIEC yield the same result regarding the content of the vesicles but there are slight differences in the frequency of observed events. Also, in VIEC a 33  $\mu\text{m}$  in diameter disk electrode is most commonly used, unlike IVIEC where a flame-etched 5  $\mu\text{m}$  carbon fiber with nanometer tip diameter is used as the electrode. In IVIEC, the flame-etched electrode has a sharp tip with size smaller than 50 nm. This geometry allows the electrode to be pierced into the cytoplasm of a living cell and facilitates quantification of the content of individual vesicle *in situ*.

In IVIEC the cell is treated as an intact system, which makes it possible to monitor the cellular response to vesicle loading with respect to external factors like osmolarity, pH, and pharmaceutical treatments with minimal impact on the cell. Whereas, in VIEC the environment surrounding the vesicles can be fully manipulated, which allows the response to vesicular loading with respect to its direct environment to be studied.<sup>146-150</sup>

### 4.1.3 Fast-Scan Cyclic Voltammetry

Fast-scan cyclic voltammetry (FSCV) is a technique commonly used for *in vivo* measurements of electroactive molecules like dopamine, norepinephrine and serotonin.<sup>9,151</sup> The main advantage of voltammetric techniques like FSCV over amperometry is the information obtained from the voltammograms. The amplitude of the anodic (oxidation) and cathodic (reduction) peaks corresponds to the concentration of the relative species. Chemical information can also be obtained from the shape of the voltammograms, since every molecule has unique redox properties, and thus information about the identity of the molecules under investigation can be obtained. By use of multivariate analysis methods, like principle component regression concentration, fluctuations of overlapping signals from *e.g.* dopamine and pH can be resolved.<sup>152</sup> A major drawback of FSCV is that significant time must be spent on scanning the potential to be able to obtain the chemical information, which thus limits the temporal resolution. This can be circumvented to some degree by increasing the scan-rate, an inherent issue, however, is that the *capacitive* current (the background) is directly proportional to the scan-rate, while the peak current (*faradaic* current) scales to the square-root of the scan-rate. In practice, what happens is that the background current saturates the amplifier causing sensitivity issues, this can be solved using analog background subtraction (ABS), with circuitry that subtracts the background (*capacitive* component) before amplification of the signal. In contrast, digital background subtraction is conventionally used when the background is within the limits of the amplifier. The use of ABS allows scan-rates as high as 2400 v/s (compared conventional 200 to 400 v/s) typically used for *in vivo* measurements.<sup>153</sup>

#### 4.1.4 Capacitance Measurements

The patch-clamp technique was developed by Bert Sakmann and Erwin Neher around 1976 to 1981, mainly as an improvement of the sharp electrode technique. In patch-clamp, a pulled glass pipette is used to create an interface between the recording instrument and a cell. Sakmann and Neher had recognized that if they could increase the seal resistance ( $R_s$ ) to the range of giga ohms the limiting *Johnson noise* would be sufficiently reduced to facilitate current recordings of single ion channels. They achieved giga ohm resistances by altering the geometry of the pipette and applying a light suction to establish a tight seal between the patch-pipette and the cell membrane.<sup>154</sup> In 1991, they were awarded the Noble Prize in physiology for their pioneering work on single ion channel recordings.

Several variations of the basic technique exist of which the *cell-attached* and *whole-cell* configuration are the two most common. The *cell-attached* is as described above, where a giga seal is established between the patch pipette and the cell of interest, allowing a small region (patch) of the cell surface to be monitored in high-resolution (low noise). Whereas, in the *whole-cell* configuration an electrical contact is established between the instrument and the cytosol of the cell, which can be obtained from the *cell-attached* configuration by the application of gentle suction pulses or electroporation. In *whole-cell* configuration the synchronous response of the whole cell is monitored rather than from a region of the membrane as in the *cell-attached* configuration.

The instrumentation used for patch-clamp recordings are often very similar and sometimes even the same as the ones used for electrochemical measurements. The patch-clamp amplifier is working in two modes either voltage-clamp or current-clamp. In the current-clamp mode the current is controlled (*clamped*) while the voltage is monitored. In contrast, in the voltage-clamp mode, the voltage is controlled meanwhile the current is monitored. One type of recording that have been used extensively in the studies of exo- and endocytosis is the *capacitance measurements*.

The simplest form of *capacitance measurements* is the time-domain technique, where the potential (voltage) is stepped according to a square-wave shaped waveform vs. time. The current response under those conditions can be described by a simple exponential equation as,

$$i(t) = i_0 * \exp^{-t/\tau} \quad \text{Eq. 34}$$

and the time-constant  $\tau$  can be expressed as,

$$\tau = C_m \times (R_A + R_m) \rightarrow C_m = \frac{\tau}{(R_A + R_m)} \quad \text{Eq. 35}$$

where  $C_m$  is the membrane capacitance,  $R_A$  is the access resistance and  $R_m$  is the resistance of the cell membrane. Changes in membrane capacitance ( $C_m$ ) as a function of time can be obtained by sequential non-linear regression of the step responses, analogous to the chronoamperometry described in *section 3.2*. These measurements allow the tracking of membrane surface area since this is proportional to the membrane *capacitance*. During *endo-* and *exocytosis*, the membrane surface area is altered and this can be observed as changes in the *capacitance*.<sup>155</sup>

In 1997, Albillos *et. al.* reported a new technique called patch-amperometry that is a hybrid of *capacitance measurements* and *single cell amperometry*. It was achieved by placing a carbon fiber micro electrode inside of a patch-pipette close enough to the patched cell membrane to achieve electrochemical recording of single release events. Simultaneously to the electrochemical recordings, high-resolution capacitance measurements can be conducted allowing information about vesicle size to be obtained simultaneously with quantitative information of the amount released.<sup>81</sup>

## 4.2 Imaging Methods

### 4.2.1 Fluorescence Microscopy

#### 4.2.1.1 Theory

In life-sciences in general, *fluorescence microscopy* proved to be a highly valuable tool for monitoring vesicular transport processes, such as *endo-* and *exocytosis*, with high spatial resolution. With *fluorescent* microscopy techniques, electromagnetic radiation (*photons*) are used to increase the energy of the *fluorophore* from its *ground state* to an *excited state*. The *excited state* is in general short lived (nanoseconds) and when the *fluorophore* returns to its ground state a photon is emitted. The emitted photon is of lower energy (longer wavelength) than the adsorbed photon causing the excitation. This is due to non-radiative energy losses, usually in the form of heat (vibrational relaxation), during the excited state lifetime. The excitation and emission wavelengths are highly dependent on the fluorophore of interest but many fluorophores used for life science research have excitation wavelengths in the range between 340 to 600 nm, which corresponds from UV to the green-yellow range of the visible spectra. Meanwhile, the wavelength of the emission is often in the range 400 to 750 nm, which correspond to violet range of the visible spectra to *near-infrared* (NIR).

#### 4.2.1.2 Fluorescent Probes

A group of fluorophores that have played a crucial role in the field of biology the last two decades are the fluorescent proteins (FPs). Many of the FPs available today are derivatives of the green fluorescent protein (GFP), for which Osamu Shimomura, Martin Chalfie and Roger Y. Tsien were awarded the Nobel Prize in 2008. The first report of GFP was made by Shimomura *et. al.* in 1962, when they successfully purified and isolated GFP from the tissue of the Jellyfish *Aequorea Victoria*, it was later also isolated from the sea pansy *Renilla reniformis*.<sup>156</sup> In 1992, the *Aequorea* GFP was successfully cloned by Prasher *et. al.* and two years later in 1994 it was used to track gene expression in *Escherichia coli* and the in nematode *Caenorhabditis elegance*.<sup>157,158</sup> In the same year (1994), Roger Y. Tsien and co-workers reported on the molecular function of the chromophore of GFP as well as an improved version of the *Aequorea* GFP. In 1995 the same group also reported a blue emitting version, which was followed over the next 10-15 years by a vast number of mutations with emission wavelengths spanning the whole visible spectra.<sup>159-163</sup>

The particular usefulness of FPs lies in the possibility to create fluorescently tagged versions of a protein of interest, a so-called fusion protein. This is done genetically by creating genetic instructions in the form of DNA or RNA, which are then introduced to the cell by a process called transfection. As a result of a successful transfection the cell is *expressing* the *fluorescently* labeled

version of the protein of interest (the fusion protein), which in most cases keeps its native function and can be tracked visually by *fluorescence microscopy*. Two such proteins that are commonly used to monitor exocytosis are enhanced green fluorescent protein labeled neuropeptide Y (EGFP-NPY) and synpato-pHluorin, which is a fusion protein of synaptobrevin and pHluorin.<sup>72</sup> EGFP-NPY is commonly used as a marker for large dense core vesicles, due to the storage of NPY in those types of vesicles. EGFP, as the name suggests, is an improved version of the *Aequorea* GFP with a chromophore mutation making EGFP 35 times brighter than the wild-type GFP. Synapto-pHluorin, is also a commonly used marker for vesicles, but is not exclusively used for large dense core vesicles as it also works for clear synaptic vesicles. Since, synaptobrevin (*syb*) (also called VAMP) is a SNARE protein essential for exocytosis (as described in section 2.2) and is generic for all vesicles, the pHluorin tag is attached to the C-terminus on the luminal side, causing the pHluorin tag to be on the inside of the vesicle. The pHluorin tag is another example of a GFP derived FP, which has been modified to become pH-sensitive with no fluorescence at pH values below 6 and bright fluorescence at physiological pH (7.4). As described earlier, the pH inside of a vesicle is around 5.5 under resting conditions and 7.4 during exocytosis. As a consequence, the pHluorin tag acts as an excellent reporter of vesicle fusion, which is also capable of reporting on the closure of the fusion pore, seen as a decrease in fluorescence as the vesicle regains its low pH. Due to the capabilities to report on pore closure, it can provide important information about release modes, such as kiss-and-run exocytosis and partial release.

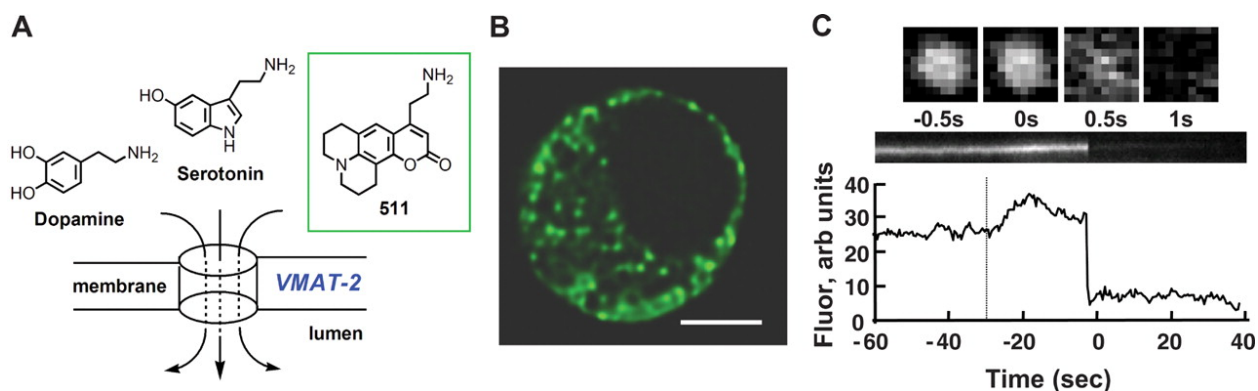


**Figure 11** (A) shows the loading of FFNs into the vesicular lumen through VMAT. (B) is a fluorescent microscopy image where loaded vesicle is clearly observed as puncta of increased fluorescence intensity. In (C) the time course of a release event observed with fluorescence microscopy, the release is observed as a sharp drop in the measured fluorescent intensity. Reprinted with permission from ref 165.

Another important group of fluorescent probes is the fluorescence false neurotransmitters (FFNs) developed by Dalibor Samos and Sulzer in 2009.<sup>164</sup> The idea of FFNs was to construct a fluorophore with structural properties similar to the neurotransmitter dopamine. The FFNs are based on a coumarin scaffold with an aminoethyl group like the catecholamines and various

substituents to tune its fluorescent properties. The aminoethyl group functions as a recognition element for the vesicle monoamine transporter (VMAT), which facilitates active uptake and accumulation in secretory vesicles inside dopaminergic neurons as well as endocrine cells like chromaffin and PC12 cells.<sup>165,166</sup> The principle of a fluorescence microscopy recording of exocytosis, using FFN is illustrated in Figure 12. FFNs are a good compliment to the FPs for studies of the exocytotic process, as they serve as reporters of small molecule content in vesicles and FPs serve to show the proteinic content. This is especially important in large dense core vesicles where proteins/peptides and small molecules are co-stored, but not always co-released.

#### 4.2.1.3 Total Internal Reflection Microscopy

*Total internal reflection fluorescence* (TIRF) microscopy is a powerful fluorescent microscopy technique that has been heavily used in the study of *exocytosis*. The total internal reflection phenomena occur when an excitation light beam is used to illuminate a solid surface (*e.g.* glass coverslip) at an angle larger than the so called *critical angle*. At an incident angle, larger than the *critical angle* all incident light is reflected and nothing is refracted (passed) through the surface. When the light gets reflected a thin electromagnetic field of the same frequency as the incident light is generated. The field is called the *evanescent field* and extends into the solution. This *field* is capable of exciting *fluorophores*, but the intensity of the field exponentially decays as a function of the distance from the surface. Therefore, only fluorophores very close the surface can be excited, which drastically reduces the background signal. Since, only molecules and events close the plasma membrane of the cell are of interest in exocytosis, TIRF microscopy is ideal for measuring and tracking single secretory granules during the full process of exocytosis. However, the normal frame times for TIRF are about 100 milliseconds making it somewhat slower than amperometry methods and the time of most exocytosis events.<sup>167-169</sup>

### 4.2.2 Electron Microscopy

Electron microscopy uses electrons rather than *photons* (electromagnetic radiation) to create an image of a sample of interest. The advantage of using electrons instead of photons is that the wavelength of an electron is much shorter than that of a photon, and consequently the beam of electrons can be focused to a much smaller point resulting in 3 orders of magnitude higher resolving power for *transmission electron microscopy* (TEM) compared to *confocal microscopy*. There are two types of electron microscopy commonly used in biology, the first is *scanning electron microscopy* (SEM) and the second is *transmission electron microscopy* (TEM). In SEM, an electron beam of primary electrons is rastered across the surface of the sample causing the emission of secondary electrons. The amount of secondary electrons emitted per pixel point defines the intensity of the pixel. Another when using SEM is to detect back-scattered electron (BSE) these electrons originate from the beam but are reflected back from the sample. Since, surfaces with heavier elements back-scatter electrons more strongly than lighter elements, this can enhance the contrast of the detected beam showing different chemical compositions for the sample, rather than only topography as observed by using secondary electrons. In general, SEM imaging of biological samples benefits from some sample preparations like fixation to tolerate high vacuum and coating to increase conductivity and reduce charging. However, a special type of SEM called environmental scanning electron microscopy (ESEM) exists, allowing minimum sample preparation. The ESEM can operate at mild vacuum with water vapor in the sample chamber, which helps to take away excess charges from samples with low conductance. ESEM instruments are not capable of obtaining the same resolution as conventional SEM instruments, however.

In contrast to SEM, TEM requires extensive sample preparation often involving chemical fixation, dehydration, embedding, sectioning, and staining before imaging can be carried out. In TEM, it is the transmitted electrons that are used to construct the image, therefore the sample has to be ultrathin around 50-70 nm in thickness. To enhance contrast between different structures, heavy metals like uranium and lead are used. However, another TEM technique called cryo-EM, exists that uses cryogenic temperatures (-196°C, liquid nitrogen) to fixate the samples but also protect it from radiation damages from the electron beam. It has use particularly useful for studies of viruses and protein structures, and was used to determine the structure of haemoglobin at 3.2Å resolution. Jaques Dubochet, Joachim Frank and Richard Henderson were awarded the 2017 Noble Prize in chemistry for their work related to the development and improvement of cryo-EM.<sup>170</sup>

### 4.2.3 Imaging Mass Spectrometry

Imaging mass spectrometry (IMS) is a group of techniques that utilize energy in some form to ionize small regions (pixels) of the sample. The ions that are created during the process are analyzed by a mass analyzer, which allows images of the molecular distributions across the sample to be obtained. IMS techniques are generally considered to be label free, but under some specific circumstances isotopic labelling is required to obtain chemical information.<sup>171</sup>

Matrix assisted laser desorption ionization (MALDI) is one of the major IMS techniques. It was introduced in the late 1980's as an ionization technique for large intact molecules and has since then played a crucial role for protein analysis in the molecular biology and biomedical field.<sup>172</sup> MALDI utilizes a matrix to adsorb the energy from the laser light, which causes desorption and ionization of the sample. Under ideal conditions it is possible to obtain spatial resolution of about 1 to 10  $\mu\text{m}$ , but this is often limited by the matrix crystal size, focus of the laser beam, and lateral diffusion during the sample preparation.<sup>173</sup> Therefore, the typical spatial resolution for MALDI is typically in practice around 10 to 50  $\mu\text{m}$ .<sup>171</sup>

Another IMS technique is secondary ion mass spectrometry (SIMS), which instead of laser light uses a primary ion beam to generate secondary ions from a sample surface. Commonly used primary ion beams used are ionized liquid metals like  $\text{Bi}_3^{2+}$  or gas cluster ion beams of substances like argon and carbon dioxide. The smaller molecular beams like  $\text{Bi}_3^{2+}$  have the advantage that they can be focused down to  $< 100 \text{ nm}$ . In contrast, large gas cluster beams of substances like  $\text{Ar}_{4000}$  can typically to date only be focused to around 2  $\mu\text{m}$ .<sup>174</sup> SIMS is a very surface sensitive method, which means that the majority of the secondary ions produced come from less than 10 nm away from the sample surface. The use of gas cluster beams like  $\text{Ar}_{4000}$  spreads the kinetic energy over many more atoms (4000 compared to 3 for  $\text{Bi}_3^{2+}$ ), which reduces the penetration depth of the primary ion into the sample. As a consequence, the generation of secondary ions is enhanced and fragmentation reduced, which facilitates detection of larger and/or more intact molecules. So far what has been described is under *static* conditions meaning that the ion dose is kept low ( $< 10^{13}$  ions/cm<sup>2</sup>). Under these conditions less than 1% of the top surface atoms receives an ion impact and *static* SIMS can be said to be virtually non-destructive.<sup>175</sup>

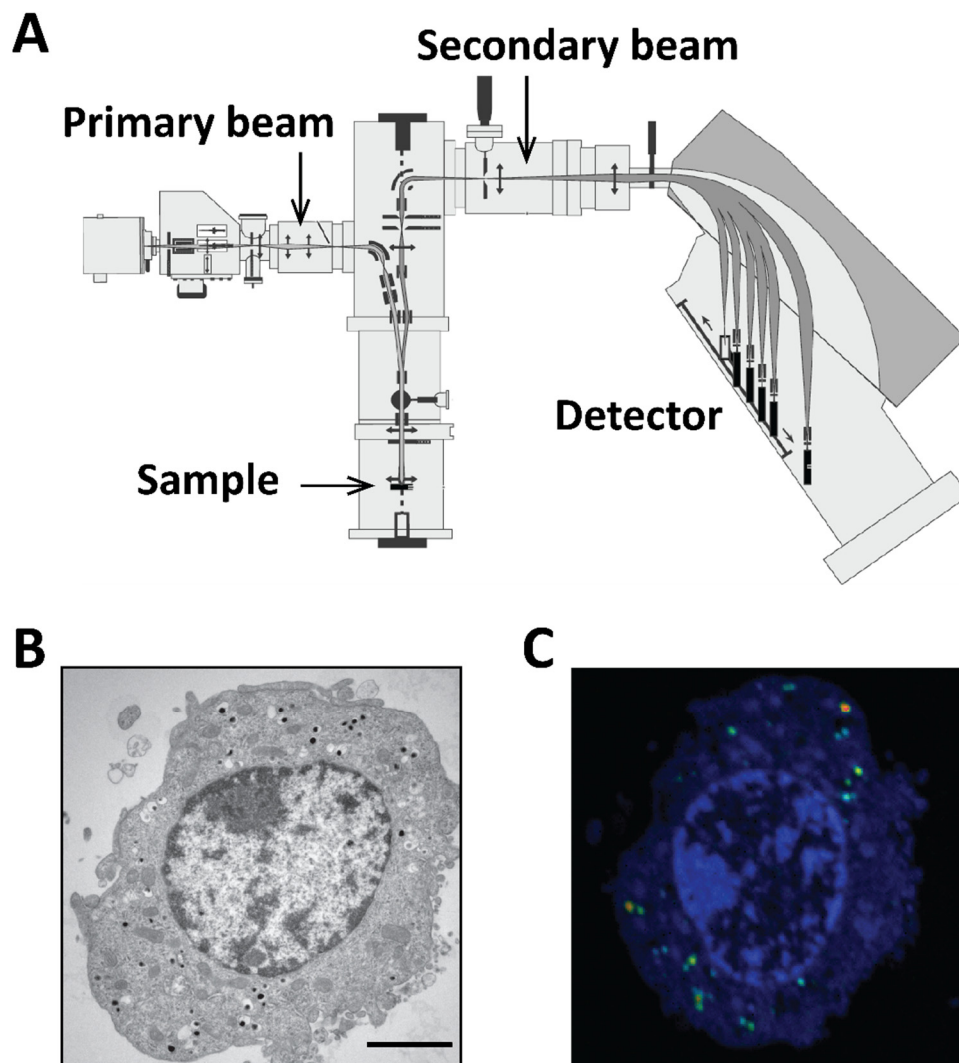


**Figure 12** In (A) a schematic of the NanoSIMS 50 (dynamic SIMS instrument), with the sample location, detector, primary and secondary beam. In (B) is an electron micrograph of a chromaffin cell and in (C) a SIMS image of the same cell, showing vesicle enrichment with  $C^{13}$ .

*Dynamic SIMS* (used in Paper VIII) utilizes high ion doses of reactive primary ion beams like  $Cs^+$  or  $O^-$ . The use of such beams causes severe fragmentation down to the atomic level, but facilitates large secondary ion yields of elements and molecular fragments. Due to the high fragmentation, stable isotope labeling (*i.e.*  $C^{13}$  and  $N^{15}$ ) of the samples is often required in order to be able to obtain useful chemical information from the samples. As a result of the very high secondary ion yield, a spatial resolution below 50 nm can be obtained with *dynamic SIMS*. This is often currently done with a NanoSIMS instrument and Figure 14 shows a schematic of the function of this instrument with images obtained to observe nanometer vesicles with TEM and compared to NanoSIMS. This is discussed more in **paper VII**.<sup>176</sup>

---

# 5 Simulations

---

## 5.1 Random-Walk

*Random-walk* (RW) simulations are a simple type of simulations, yet they are capable of predicting the outcome of complex systems in a range of different fields like for example, economics, biology, physics, and chemistry. An example of the Random Walk method is shown in Figure 15. This approach is commonly applied in studies of particle diffusion and Brownian motion. In this thesis work, random-walk simulations were used in paper IV to track individual particles (catecholamines) released across the cell surface to evaluate in what fraction released catecholamines from the same origin reached the different electrodes. These results were correlated with data obtained from amperometry measurements to allow visualization release distribution across a region of the cell membrane.

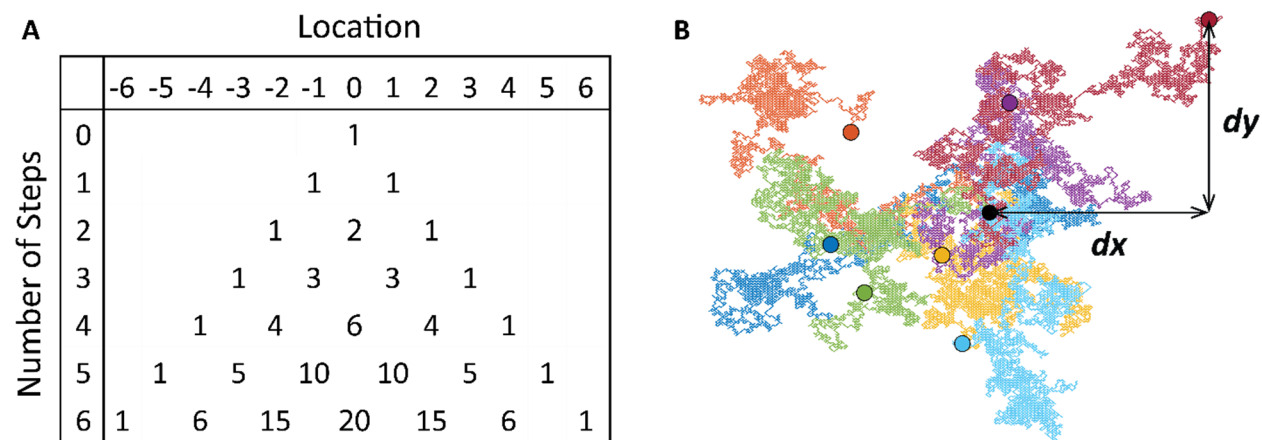


**Figure 13** In (A) is the relative population of different locations during the first 6 steps of a *random-walk* simulation. (B) shows a 2D *random-walk* simulation of 1000 steps of 7 different particles with the same origin. The **solid solid black** circle is the origin position and the colored circles are the particle position at the end of the simulation. The measurement of the displacement is illustrated by the arrow in B. where  $dx$  and  $dy$  is the displacement in the  $x$ - and  $y$ -direction, respectively.

The *random-walk* process can be described as a two-state Markov chain model with equal probability for both states; that is a particle has an equal 50% chance of going either forward (+1) or backwards (-1). If this is done in a series of step, as illustrated in *Fig. XA* the likelihood of finding a particle at the location 0 after 0 steps is 100%, which means that all particles have the same origin. Now if the simulation is stepped once, the particles that before were at the locations 0 will be distributed between location -1 and 1 at a ratio of 1:1, that is 50% went forward and 50%

went backwards. The distribution of particles in the geometry continues to become broader as the simulation is proceeding, and follows a *gaussian* distribution as shown in Figure 16A.

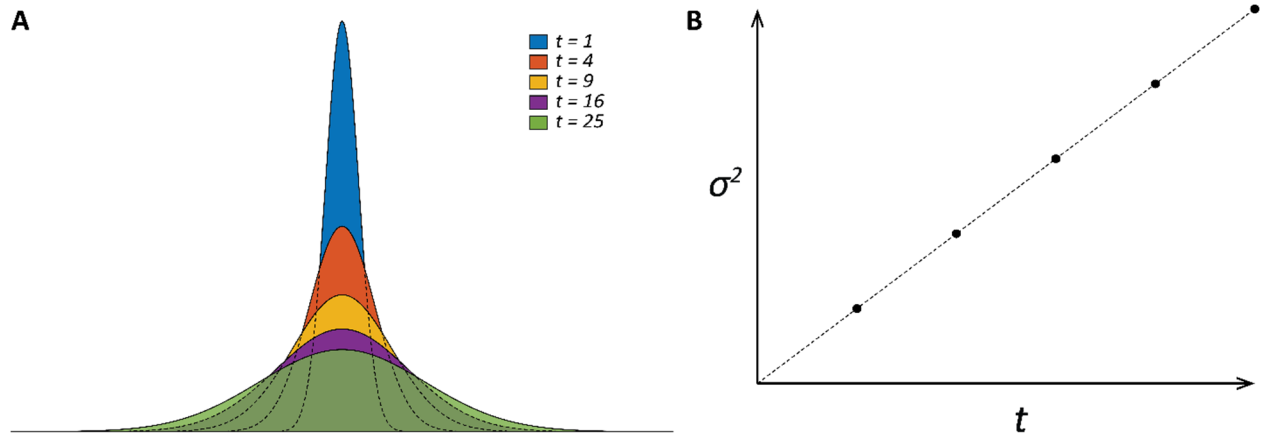


**Figure 14** In (A) the distribution of molecules a long a single dimension is shown at the time  $t$  equal to 1,4,9,16 and 25. In (B) it is shown how the *variance* ( $\sigma^2$ )of the distributions shown in A increase directly propotional to the time  $t$ . The variance ( $\sigma^2$ ) of the gaussian distribution is directly proportional to the time (number of steps). The variance is approximately the same as the *mean squared displacement* (MSD) of the particles, which can be calculated according to Eq. X.

$$\sigma^2 = \left( \frac{(dx_1^2 + dx_2^2 + \dots + dx_n^2)}{n} \right)^2 = MSD \quad \text{Eq. 36}$$

Where  $dx_i$  is the distance of particle  $x_i$  from the origin  $x_0$  and  $n$  is the number of particles. The measurement of the *displacement* for a particle in two-dimensions is illustrated in Fig XB. However, the *mean squared displacement* is related to time through the diffusion coefficient  $D$  according to following expression:

$$MSD = 2Dt \quad \text{Eq. 37}$$

This, generalized expression for diffusion is true if there are no constrains added to the model, meaning the particle is free to move anywhere along the dimensions simulated. However, constrains can be added, so called, boundary conditions, that can account for blocked surfaces, adsorption, or chemical reactions. For example, a polarized electrode held at a large overpotential can be simulated as a sink, by allowing particles to exit the simulation at certain coordinates. Since, the location of all particles is known at any given time of the simulation, information about where and when a particle exits the simulation can be obtained. This information can be converted to current densities and i-t responses.

## 5.2 Finite Element Method

The *finite element method* (FEM) is a numerical simulation method used in many field, such as in chemistry, physics and mechanical engineering. It is commonly used to study heat transfer, mass transport (*e.g.* diffusion), and for structural analysis. In FEM the problem is usually expressed in term of *partial-differential equations* (PDEs), which usually cannot be solved for complex geometries. Instead, an approximation of the equations can be constructed, dividing the complex geometry in to smaller segments called *finite elements* by the creation of a *mesh* (Figure 17A). The *mesh* contains a series of *nodes* that each is described by an equation. The equations for all the individual *finite elements* are combined to obtain a system of algebraic equations in a matrix, which can be solved numerically by a computer.

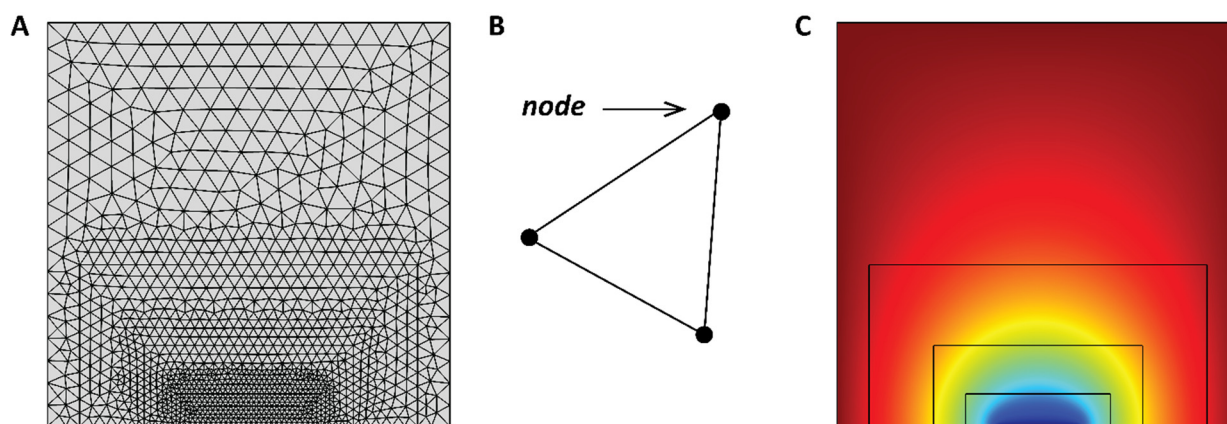


**Figure 15** In (A) a geometry for FEM simulation is shown with the *meshing grid* defining the *finite elements*. (B) shows how the *meshing grid* is constructed, with three *nodes* as in the case of a triangular *mesh*. In (C) the solution of a FEM simulation of the *steady-state* concentration of a *species C* in the presence of polarized electrode is shown. The color scales the concentration from *dark blue* (low) to *dark red* (high).

The solution, for example of a mass transport problem as described in Figure 17C is a value for the concentration at each *node*. By knowing the value at the *nodes*, the concentration at any other point in the geometry can be obtained by interpolation. This further can be used to obtain fluxes, which can be converted into currents to simulate electrochemical problems.<sup>177</sup>

## 5.3 Conclusion of Simulation

The two simulation methods describe here, the *random-walk* (RW) and the *finite-element method* (FEM) both have in common that a large amount of iterations are required to solve the problems of interest. One possible limitation of RW simulations is that the step size ( $m$ ) is intrinsically linked to the time step ( $s$ ) through the diffusion coefficient ( $m^2/s$ ). For example, with a step size of  $1 \times 10^{-9} m$  (1 *nm*) and a diffusion coefficient of  $7.3 \times 10^{-11} m^2 s^{-1}$  (as for dopamine during exocytosis) each step corresponds to 6.85 *ns*; and to simulate an *exocytotic* event with a time span of 150 *ms* would require around 22 million iterations. Additionally, since the RW method relies on a statistical approach rather than a numerical one, a large number of particles have to be simulated (>10,000 particles) to obtain acceptable results. The simplicity and flexibility in combination with the possibility of particle-tracking is the strength of RW simulations.

The FEM, however, does not put any constraints on the time-steps used, and in fact logarithmic stepping can easily be implemented (which is very useful for simulations of exocytosis). The quality of the solution in FEM is related to the *nodes* of the *mesh*, the more *nodes* and finer *mesh* used the better the solutions obtained at the cost of computation time. Also, multiple simulations of the same geometry must be carried out in order to verify the stability of the obtained solution. However, FEM allows higher complexity both in terms of the problem itself and the geometry to be simulated.

---

## 6 Summary of Papers

---

My work has focused on amperometric measurements of exocytosis and the contents of vesicles, as well as some ancillary methods in mass spectrometry. I have spent most of my time working on collaborative efforts in these measurements and to model the results with simulations. The production of multi-electrode arrays (MEAs) consisting of 16, 25 or 36 individually addressable platinum electrodes was demonstrated in **paper I**. Individual electrode of dimension down to  $2 \times 2 \mu\text{m}$  was achieved, which allowed the exocytotic activity at a single PC12 cells to be recorded at 8 electrodes simultaneously. From these recording, heterogeneous activity of exocytosis was clearly observed, which supports the hypothesis that exocytotic release take place at hot-spots across the cell surface. A key aspect to understand exocytosis measurements is to have the ability to quantify the content of vesicles that undergo exocytosis.

In **paper II**, I proposed a new methodology to quantify the content of individual vesicles. The methodology was initially called vesicle electrochemical cytometry (VEC) but was later modified to be called vesicle impact electrochemical cytometry (VIEC). It was demonstrated that isolated chromaffin vesicles adsorb onto the carbon electrode surface to build up a population of vesicles that eventually rupture stochastically to release their contents one at a time in very close proximity to the electrode surface. These rupture events are observed as current transients very similar to those observed during single cell amperometry recordings of exocytosis. By integration of the current transients it was found that an average bovine chromaffin vesicle contains about  $4.3 \times 10^6$  catecholamine molecules, which when tentatively compared to previous reported values in the literature, indicated that approximately 42% of the content of each vesicle was released during an average exocytotic event. Furthermore, the size distribution of the isolated vesicles has been measured with nanoparticle tracking analysis (NTA), and it has been found that the concentration calculated based on average vesicle radius and charge integral (Q) can be used to reconstruct the vesicular size distributions from the electrochemical measurement with the assumption that the concentration of catecholamine was equal in all vesicles.

The VIEC methodology led to a new approach for to quantify the content of vesicles inside living cells. This is called intracellular vesicle impact electrochemical cytometry (IVIEC) and was introduced in **paper III**. In IVIEC, a cylindrical carbon fiber electrode is flame-etched to create a conically shaped electrode that is used to penetrate the plasma membrane to access the cytoplasm of a living cell. In the cytosol the vesicles impact, adsorb, and rupture at the electrode surface, similarly to what is observed outside the cell in VIEC. This allows the vesicular content to be quantified in situ. By using the same electrode for both exocytosis (SCA) measurements and

IVIEC to measure content of the vesicles, a fraction of the release could be estimated for PC12 cells with same signal to noise ratio. It was found that the vesicles contained on average 115,000 molecules and on average 73,200 molecules were released per exocytotic event. This indicates that on average 64% of the vesicular content is released per event in PC12 cells. The same measurements were also carried out after incubation with L-DOPA and it was found that the amount released and the vesicular content increased to 329,100 and 209,000, respectively. The fraction of release for L-DOPA treatment was almost identical that of the control, 65% for L-DOPA vs. 64% for the control. It was concluded that L-DOPA is strongly affecting the amount released and the vesicular content without alter the fraction released. Furthermore, the result that around 65% of the content is released both during L-DOPA treatment and under control conditions was taken as strong support for the concept of open and closed exocytosis. To fully understand and quantify VIEC and IVIEC measurements, it is necessary to develop a mechanism of the vesicle opening.

To investigate the mechanism of vesicular rupture at the electrode surface during VIEC, a bottom-up approach comparing liposomes, peptide decorated liposomes and chromaffin large-dense core vesicles, was used in **paper VI**. It was proposed that rupturing mainly happened through electroporation. This was supported by the observation of an increased event frequency as a function of the applied potential. It was estimated that the electric field was in the range of  $1.4 \times 10^6$  V/cm<sup>2</sup> for a vesicular membrane within the distance (around 5-10 nm) of the double layer from the electrode surface. To test the hypothesis if the proteins of the vesicles could act as a physical barrier of electroporation, liposomes were compared to peptide-decorated liposomes. It was observed that the peptides significantly reduced the time course of the rupturing events, and that the rupture of liposomes was twenty times more efficient than that of chromaffin vesicles. This strengthens the concept that peptides/proteins act as a physical barrier to the membrane contacting the electrode surface. It is hypothesized that these proteins must diffuse away from the vesicle-electrode contact area before electroporation can occur.

In **paper V**, the effect of excited fluorophores on the opening of vesicles during VIEC measurements is described to further understand the mechanism of vesicle opening in VIEC. It was observed that vesicles labeled with Rho-PE or NBD-PE, significantly increased the frequency of vesicle rupture events when stimulated with light at the fluorophore excitation wavelength. The effect was both dependent on the intensity of the light and the concentration of fluorophore. The observed effect was speculated to be a result of the production of reactive oxygen species by the excited fluorophore. This was tested by the addition of H<sub>2</sub>O<sub>2</sub> or DMSO, which both showed similar effects as observed in the present of excited fluorophores. The observed effect was

attributed the oxidation of the membrane lipids, leading to a reduced thickness of the membrane and increased electroporation efficiency.

Further investigation of the mechanistic aspects of vesicle rupture during VIEC was done in **paper IX**. It was observed that an increase in the temperature both led to increased frequency of the observed events but also sped up the time course of individual events, indicating an increase in the efficiency of electroporation as well as the formation of a larger pore. It was also noted that large vesicles appear to open more efficiently, this was demonstrated by increasing and decreasing the size of the vesicles pharmacologically with L-DOPA and reserpine, respectively. A increased diffusion rate of the vesicular membrane proteins with temperature and an increased exposure of the membrane with size was hypothesized to cause the increased efficiency of electroporation.

The mechanistic models developed in the papers V, VI and IX provided confidence that we could accurately quantify the contents of vesicles in the VIEC and IVIEC shown in papers II and III. In **paper VII**, the storage mechanism of catecholamines in the large dense-core vesicles of PC12 cells was studied by the use of pharmacologically treatments of L-DOPA and reserpine. A novel method to image and spatially resolve the chemistry of isotopically labeled dopamine across single vesicles with a dynamic SIMS instrument (NanoSIMS) was presented. The combination of NanoSIMS with IVIEC facilitated correlations between the relative quantification of NanoSIMS with the total quantification of the vesicular content from IVIEC. It was observed that the redistribution of dopamine between different vesicular compartments, dense-core and halo, is a kinetically limited process. The slow redistribution between the compartments might have important regulatory functions during dopamine storage and release. All these studies of vesicles opened new concepts to study relative to exocytosis.

Thus, in **paper VIII** the effect of dimethyl sulfoxide (DMSO) on exocytosis was studied. DMSO is commonly used in many biological studies due to its excellent ability to solubilize many therapeutic agents. However, little is known about the effects of DMSO on its own. To study this, PC12 cells were incubated with a series of concentrations from 0 to 1% DMSO. After incubation with 0.6% DMSO a significant increase in the risetime,  $I_{max}$ , as well as the number of molecules released, and the duration of the pre-spike foot was observed. These observations were attributed to the permeabilization and thinning of the membrane by DMSO, leading to increased pore stability.

In **paper IV** I was involved in a collaborative project to develop a new approach to spatially measure exocytosis across the top of cells with an MEA. Instead of culturing the cells on top of the electrode array as done in paper I, the fabricated arrays were diced and polished to a sharp tip around the electrode area. This approach permits positioning of a micro-fabricated probe on top of a cell and to carry out amperometric recordings of the exocytotic activity, leading to a significant improvement of the workflow by increasing the number of possible measurements per probe. The geometry of the MEA with 16 individually addressed platinum band electrodes distributed in 8 rows and 2 columns that were confined to a 20x25  $\mu\text{m}$  area, allowed detailed information about the magnitude and location exocytosis across the cell surface. Amperometric data were collected and correlated with random-walk simulations allowing both 1D and 2D distribution of the exocytotic activity to be obtained, which allowed hot-spots of activity to be observed, with a spatial distribution less than 120 nm.

In summary, the work in this thesis is a combination of new methods to measure exocytosis release and the content of vesicles purified and in situ and the application of these methods to understand transmitter storage and exocytosis.

---

## 7 Concluding Remarks and Future Outlook

---

The process of exocytosis allows cells to communicate with each other following an input by either a direct action or by further propagating the signal forward. It is the key process through which cell-to-cell communication takes place and is essential for all life. The work in this thesis is aimed to develop methods that can further extend our knowledge about how exocytosis is regulated down to the vesicular level. In papers II and III, I have demonstrated two new approaches that allow the vesicular content of isolated vesicles (*in-vitro*) and in the cytosol of live cells (*in-situ*). These two approaches are highly complementary, as the isolation of vesicles facilitates full control of the surrounding environment of the vesicle allowing direct effect on vesicular loading to be studied. Measurements in live cells allow the cellular response to external factors such as for example, toxins, drugs, and stress, on vesicular loading to be measured. Also, the quantification of the vesicular content in live cells can be directly compared with the amount released during exocytosis by amperometric measurements from cells of the same culture.

The two methods described above both rely on the same principle, vesicle rupture in close proximity to an electrode surface to release its content, which is then transported from the inside to the electrode by diffusion. The catecholamine content of the vesicle is rapidly detected through oxidation after reaching the surface of the electrode. Combined QCM-D and electrochemical measurements were initially used, followed later by scanning electron micrographs to demonstrate that adsorption was a key factor in the VIEC process. Adsorption of vesicles allows accumulation at the electrode surface prior to rupture and detection. The mechanistic aspects of these two methods were studied and are described in paper V, VI, and IX. It was found that the rupturing efficiency could be increased by an increase in either the applied potential or the temperature, but also with perturbation of the vesicular membrane by the direct addition of hydrogen peroxide or its generation through excitation of introduced fluorophores to the vesicles. Also, perturbation of the membrane can be achieved by the addition of DMSO or by increasing the size of the vesicles by L-DOPA-induced loading. Factors affecting the efficiency of rupturing have been quite extensively studied as described above, but the prior steps of adsorption are known to a lesser extent. This was illustrated by the fact that a 20x frequency of rupturing events was observed with liposomes compared to chromaffin vesicles at the same concentrations of each. To study this further the combination of TIRF microscopy and electrochemistry could be used, by labelling the content and/or the vesicular membrane the transport towards the electrode as well as the adsorption process itself might be studied. In the future, this approach might be used to examine the adsorption efficacy, vacancy times at the

electrode surface, diffusion coefficients corresponding to vesicular size all simultaneously with the electrochemical observation of rupture efficiency.

To further expand our knowledge about the factors underlying vesicular loading and storage of catecholamines, we combined three techniques including dynamic SIMS, transmission electron microscopy, and electrochemistry to study can compare vesicular content and structure. The combination of dynamic SIMS and transmission electron microscopy allowed chemical distributions of catecholamine inside the cell to be correlated with ultra-structures observed in electron micrographs. This further allowed the distribution of isotopic labelled dopamine between the two compartments of the vesicle, halo and dense-core, to be measured after pharmacological treatment with reserpine and L-DOPA. The correlation of the relative quantification with NanoSIMS with the absolute quantification obtained by electrochemistry in combination with ultra-structural information from the micrographs revealed kinetic limitations for dopamine redistributions within the closed vesicle. This methodology can be further extended to study the effect of a wide range of drugs and their direct effects on loading and storage of catecholamines in vesicles.

Two examples of electrochemical imaging with multi electrode arrays (MEAs) are described in papers **I** and **IV**. The same basic method of fabrication was used in both papers and included steps like lithography and thin film deposition to produce a pattern of platinum micro-wires on a borosilicate surface. The larger part of the wires was subsequently insulated to obtain clearly defined electrode areas. In paper **I**, it is demonstrated that 36 (6x6) individually addressable electrodes can be fabricated with individual electrode size of 2x2  $\mu\text{m}$ . This platform was successfully used to monitor the exocytotic release from a single PC12 cell with 8 electrodes simultaneously. The results were used to show the spatial distribution of exocytotic activity as a function of time, and a clear heterogenous activity across the foot print of the cell was observed. In paper **IV**, another new approach was demonstrated, by dicing and beveling of the MEA, could confine the electrodes to a sharp tip. This new geometry of MEA made a probe that could be used to approach a cell from above compared to conventional cell culture on top of the MEA (as in paper **I**). The fact that the new MEA probe could be used in similar way as carbon fiber electrode significantly increased the workflow by allowing measurement from multiple cells by the same probe. The size of the individual electrodes was pushed to the limit of the lithography process and band electrodes with a width of around 1  $\mu\text{m}$  were achieved. The decreased size of the individual electrodes allowed 16 electrodes to be used simultaneously during single cell recordings. The electrode geometry further allowed 2D imaging of the exocytotic activity across a sub region of the cells surface. The electrochemical imaging between adjacent electrodes could

be obtained by assigning the origin of the exocytotic events to a pixel point by correlating the amperometric response to random-walk simulations. This approach allowed hot-spots in the size of 120 nm to be observed and spatially resolved at chromaffin cells.

In conclusion, new electrochemical methods have been developed, allowing the effects on vesicle loading and storage prior exocytosis to be studied and the information gained to be directly correlated with recordings of the release. This can potentially provide important information about the regulatory mechanism prior, during, and after exocytosis. In combination with high resolution chemical imaging (dynamic SIMS) and electron microscopy, important information about the sub-vesicular distribution can be obtained expanding our knowledge of how the ultrastructure of secretory vesicles is involved in the regulation of exocytosis.



---

## 8 Acknowledgements

---

I started as a master student in the group in 2011 and since then I have met a lot of people that have been very important for me personally and scientifically to grow as a person and for that I want to acknowledge them.

First of all, I would like to thank my supervisor **Andrew Ewing** for giving me the opportunity, guidance and support to allow me to pursue a PhD, and for always being available when needed. I am also truly grateful for all the freedom to try new things and allowing me to travel to conferences and courses throughout the years.

To my semi-supervisors **John** and **Per**, for being almost perfect lunch mates.

To **Jenny**, for endless electrochemistry discussions and for following me through the PhD. Also showing that everything is possible.

To **Lisa** and **Mike**, for introducing me to science, all the collaborations and for the friendship throughout the years.

To **Ibrahim** for the constant ongoing scientific discussions and for teaching me Turkish history and world politics.

To **Joakim** for all inspiring side-tracks, making the PhD slightly more interesting.

My office-mates **Laura** and **Mai**, for great companionship and snacks.

The present members of the **Ewing, Fletcher, Cans, Hanrieder** and **Safina** research groups, Soodi, Anna, Xian, Zahra, Sanna, Mary, Alex, Pieter, Shoko, Amir M, Elias, Mohaddeseh, Amir H, Marwa, Kelly, Chaoyi, Wanying, Daixin, Lin, Florent, Yuanmo and all the past members of the groups for all great group meetings, social activities, and coffee room discussions providing a nice working environment throughout the years.

I also want to send a special thank you to all **co-authors** of the manuscripts for all interesting collaborations and discussions.

To all the people at floor 4, 5 and MC2 for providing a nice working environment and always being available to help when needed.

Till Elin och Melvin, för att ni alltid finns där. Älskar er!

Tack mamma för att du trodde på mig, och pappa för att du introducerade mig till kemin!



---

## 9 References

---

1. KANDEL, E. R., SCHWARTZ, J. H., & JESSELL, T. M. (2013). PRINCIPLES OF NEUROSCIENCE, 5TH.
2. ALBERTS, BRUCE. MOLECULAR BIOLOGY OF THE CELL. GARLAND SCIENCE, 2017.
3. BRADY, S., SIEGEL, G., ALBERS, R. W., & PRICE, D. (EDS.). (2011). BASIC NEUROCHEMISTRY: PRINCIPLES OF MOLECULAR, CELLULAR, AND MEDICAL NEUROBIOLOGY. ACADEMIC PRESS.
4. HEIDELBERGER, R., HEINEMANN, C., NEHER, E., & MATTHEWS, G. (1994). CALCIUM DEPENDENCE OF THE RATE OF EXOCYTOSIS IN A SYNAPTIC TERMINAL. NATURE, 371(6497), 513.
5. CARLSSON, A., LINDQVIST, M., & MAGNUSSON, T. O. R. (1957). 3, 4-DIHYDROXYPHENYLALANINE AND 5-HYDROXYTRYPTOPHAN AS RESERPINE ANTAGONISTS. NATURE, 180(4596), 1200-1200.
6. CARLSSON, A. (1959). THE OCCURRENCE, DISTRIBUTION AND PHYSIOLOGICAL ROLE OF CATECHOLAMINES IN THE NERVOUS SYSTEM. PHARMACOLOGICAL REVIEWS, 11(2), 490-493.
7. SCHULTZ, W. (1997). DOPAMINE NEURONS AND THEIR ROLE IN REWARD MECHANISMS. CURRENT OPINION IN NEUROBIOLOGY, 7(2), 191-197
8. GIROS, B., JABER, M., JONES, S. R., WIGHTMAN, R. M., & CARON, M. G. (1996). HYPERLOCOMOTION AND INDIFFERENCE TO COCAINE AND AMPHETAMINE IN MICE LACKING THE DOPAMINE TRANSPORTER. NATURE, 379(6566), 606-612.
9. WIGHTMAN, R. M., MAY, L. J., & MICHAEL, A. C. (1988). DETECTION OF DOPAMINE DYNAMICS IN THE BRAIN. ANALYTICAL CHEMISTRY, 60(13), 769A-793A.
10. AGNATI, L. F., ZOLI, M., STRÖMBERG, I., & FUXE, K. (1995). INTERCELLULAR COMMUNICATION IN THE BRAIN: WIRING VERSUS VOLUME TRANSMISSION. NEUROSCIENCE, 69(3), 711-726.
11. BENINGER, R. J. (1983). THE ROLE OF DOPAMINE IN LOCOMOTOR ACTIVITY AND LEARNING. BRAIN RESEARCH REVIEWS, 6(2), 173-196.
12. DAUER, W., & PRZEDBORSKI, S. (2003). PARKINSON'S DISEASE: MECHANISMS AND MODELS. NEURON, 39(6), 889-909.
13. CEPEDA, C., MURPHY, K. P., PARENT, M., & LEVINE, M. S. (2014). THE ROLE OF DOPAMINE IN HUNTINGTON'S DISEASE. PROGRESS IN BRAIN RESEARCH, 211, 235.
14. EULER, U. S. (1945). A SYMPATHOMIMETIC PRESSOR SUBSTANCE IN ANIMAL ORGAN EXTRACTS. NATURE, 156, 18-19.
15. EULER, U. V. (1946). A SPECIFIC SYMPATHOMIMETIC ERGONE IN ADRENERGIC NERVE FIBRES (SYMPATHIN) AND ITS RELATIONS TO ADRENALINE AND NOR-ADRENALINE. ACTA PHYSIOLOGICA, 12(1), 73-97.
16. EULER, U. V., & LILJESTRAND, G. (1946). OBSERVATIONS ON THE PULMONARY ARTERIAL BLOOD PRESSURE IN THE CAT. ACTA PHYSIOLOGICA, 12(4), 301-320.
17. WAHLESTEDT, C. L. A. E. S., HAKANSON, R. O. L. F., VAZ, C. A., & ZUKOWSKA-GROJEC, Z. (1990). NOREPINEPHRINE AND NEUROPEPTIDE Y: VASOCONSTRICTOR COOPERATION IN VIVO AND IN VITRO. AMERICAN JOURNAL OF PHYSIOLOGY-REGULATORY, INTEGRATIVE AND COMPARATIVE PHYSIOLOGY, 258(3), R736-R742.
18. ASTON-JONES, G., & COHEN, J. D. (2005). AN INTEGRATIVE THEORY OF LOCUS COERULEUS-NOREPINEPHRINE FUNCTION: ADAPTIVE GAIN AND OPTIMAL PERFORMANCE. ANNU. REV. NEUROSCI., 28, 403-450.
19. HO, T., FUXE, K., GOLDSTEIN, M., & JOHANSSON, O. (1974). IMMUNOHISTOCHEMICAL EVIDENCE FOR THE EXISTENCE OF ADRENALINE NEURONS IN THE RAT BRAIN. BRAIN RESEARCH, 66(2), 235-251.
20. VANHOUTTE, P. M., VERBEUREN, T. J., & WEBB, R. C. (1981). LOCAL MODULATION OF ADRENERGIC NEUROEFFECTOR INTERACTION IN THE BLOOD VESSEL WALL. PHYSIOLOGICAL REVIEWS, 61(1), 151-247.
21. HEMS, D. A., & WHITTON, P. D. (1980). CONTROL OF HEPATIC GLYCOGENOLYSIS. PHYSIOLOGICAL REVIEWS, 60(1), 1-50.

22. BARACH, E. M., NOWAK, R. M., LEE, T. G., & TOMLANOVICH, M. C. (1984). EPINEPHRINE FOR TREATMENT OF ANAPHYLACTIC SHOCK. *JAMA*, 251(16), 2118-2122.
23. SHIMAN, R., AKINO, M., & KAUFMAN, S. (1971). SOLUBILIZATION AND PARTIAL PURIFICATION OF TYROSINE HYDROXYLASE FROM BOVINE ADRENAL MEDULLA. *JOURNAL OF BIOLOGICAL CHEMISTRY*, 246(5), 1330-1340.
24. DAUBNER, S. C., LE, T., & WANG, S. (2011). TYROSINE HYDROXYLASE AND REGULATION OF DOPAMINE SYNTHESIS. *ARCHIVES OF BIOCHEMISTRY AND BIOPHYSICS*, 508(1), 1-12.
25. CHRISTENSON, J. G., DAIRMAN, W., & UDENFRIEND, S. (1970). PREPARATION AND PROPERTIES OF A HOMOGENEOUS AROMATIC L-AMINO ACID DECARBOXYLASE FROM HOG KIDNEY. *ARCHIVES OF BIOCHEMISTRY AND BIOPHYSICS*, 141(1), 356-367.
26. CRAINE, J. E., DANIELS, G. H., & KAUFMAN, S. (1973). DOPAMINE-B-HYDROXYLASE THE SUBUNIT STRUCTURE AND ANION ACTIVATION OF THE BOVINE ADRENAL ENZYME. *JOURNAL OF BIOLOGICAL CHEMISTRY*, 248(22), 7838-7844.
27. LAMOUROUX, A., VIGNY, A., BIGUET, N. F., DARMON, M. C., FRANCK, R., HENRY, J. P., & MALLET, J. (1987). THE PRIMARY STRUCTURE OF HUMAN DOPAMINE-BETA-HYDROXYLASE: INSIGHTS INTO THE RELATIONSHIP BETWEEN THE SOLUBLE AND THE MEMBRANE-BOUND FORMS OF THE ENZYME. *THE EMBO JOURNAL*, 6(13), 3931.
28. VENDELBOE, T. V., HARRIS, P., ZHAO, Y., WALTER, T. S., HARLOS, K., EL OMARI, K., & CHRISTENSEN, H. E. (2016). THE CRYSTAL STRUCTURE OF HUMAN DOPAMINE B-HYDROXYLASE AT 2.9 Å RESOLUTION. *SCIENCE ADVANCES*, 2(4), e1500980.
29. CONNETT, R. J., & KIRSHNER, N. (1970). PURIFICATION AND PROPERTIES OF BOVINE PHENYLETHANOLAMINE N-METHYLTRANSFERASE. *JOURNAL OF BIOLOGICAL CHEMISTRY*, 245(2), 329-334.
30. ISOBE, K., TAKEKOSHI, K., & KAWAKAMI, Y. (2004). PHENYLETHANOLAMINE N-METHYLTRANSFERASE.
31. EVINGER, M. J., TOWLE, A. C., PARK, D. H., LEE, P., & JOH, T. H. (1992). GLUCOCORTICOID STIMULATE TRANSCRIPTION OF THE RAT PHENYLETHANOLAMINE N-METHYLTRANSFERASE (PNMT) GENE IN VIVO AND IN VITRO. *CELLULAR AND MOLECULAR NEUROBIOLOGY*, 12(3), 193-215.
32. WURTMAN, R. J., & AXELROD, J. (1966). CONTROL OF ENZYMIC SYNTHESIS OF ADRENALINE IN THE ADRENAL MEDULLA BY ADRENAL CORTICAL STEROIDS. *JOURNAL OF BIOLOGICAL CHEMISTRY*, 241(10), 2301-2305.
33. EISENHOFER, G., KOPIN, I. J., & GOLDSTEIN, D. S. (2004). CATECHOLAMINE METABOLISM: A CONTEMPORARY VIEW WITH IMPLICATIONS FOR PHYSIOLOGY AND MEDICINE. *PHARMACOLOGICAL REVIEWS*, 56(3), 331-349.
34. KOPIN, I. J. (1985). CATECHOLAMINE METABOLISM: BASIC ASPECTS AND CLINICAL SIGNIFICANCE. *PHARMACOLOGICAL REVIEWS*, 37(4), 333-364.
35. POWELL, H. C., GARRETT, R. S., KADOR, P. F., & MIZISIN, A. P. (1991). FINE-STRUCTURAL LOCALIZATION OF ALDOSE REDUCTASE AND OUBAIN-SENSITIVE, K<sup>+</sup>-DEPENDENT P-NITRO-PHENYLPHOSPHATASE IN RAT PERIPHERAL NERVE. *ACTA NEUROPATHOLOGICA*, 81(5), 529-539.
36. KALARIA, R. N., MITCHELL, M. J., & HARIK, S. I. (1988). MONOAMINE OXIDASES OF THE HUMAN BRAIN AND LIVER. *BRAIN*, 111(6), 1441-1451.
37. KAWAMURA, M., EISENHOFER, G., KOPIN, I. J., KADOR, P. F., LEE, Y. S., FUJISAWA, S., & SATO, S. (2002). ALDOSE REDUCTASE: AN ALDEHYDE SCAVENGING ENZYME IN THE INTRANEURONAL METABOLISM OF NOREPINEPHRINE IN HUMAN SYMPATHETIC GANGLIA. *AUTONOMIC NEUROSCIENCE*, 96(2), 131-139.
38. KAWAMURA, M., EISENHOFER, G., KOPIN, I. J., KADOR, P. F., LEE, Y. S., TSAI, J. Y., ... & SATO, S. (1999). ALDOSE REDUCTASE, A KEY ENZYME IN THE OXIDATIVE DEAMINATION OF NOREPINEPHRINE IN RATS. *BIOCHEMICAL PHARMACOLOGY*, 58(3), 517-524.
39. KARHUNEN, T., TILGMANN, C., ULMANEN, I., JULKUNEN, I., & PANULA, P. (1994). DISTRIBUTION OF CATECHOL-O-METHYLTRANSFERASE ENZYME IN RAT TISSUES. *JOURNAL OF HISTOCHEMISTRY & CYTOCHEMISTRY*, 42(8), 1079-1090.
40. CHEN, J., LIPSKA, B. K., HALIM, N., MA, Q. D., MATSUMOTO, M., MELHEM, S., ... & EGAN, M. F. (2004). FUNCTIONAL ANALYSIS OF GENETIC VARIATION IN CATECHOL-O-METHYLTRANSFERASE (COMT): EFFECTS ON mRNA, PROTEIN, AND ENZYME ACTIVITY IN POSTMORTEM HUMAN BRAIN. *THE AMERICAN JOURNAL OF HUMAN GENETICS*, 75(5), 807-821.

41. MATSUMOTO, M., WEICKERT, C. S., BELTAIFA, S., KOLACHANA, B., CHEN, J., HYDE, T. M., ... & KLEINMAN, J. E. (2003). CATECHOL O-METHYLTRANSFERASE (COMT) mRNA EXPRESSION IN THE DORSOLATERAL PREFRONTAL CORTEX OF PATIENTS WITH SCHIZOPHRENIA. *NEUROPSYCHOPHARMACOLOGY*, 28(8), 1521.
42. TENHUNEN J, SALMINEN M, JALANKO A, UKKONEN S, ULMANEN I (1993) STRUCTURE OF THE RAT CATECHOL-O-METHYLTRANSFERASE GENE: SEPARATE PROMOTERS ARE USED TO PRODUCE MRNAs FOR SOLUBLE AND MEMBRANE-BOUND FORMS OF THE ENZYME. *DNA CELL BIOL* 12:253–263
43. DUNEVALL, J., FATHALI, H., NAJAFINOBAR, N., LOVRIC, J., WIGSTRÖM, J., CANS, A. S., & EWING, A. G. (2015). CHARACTERIZING THE CATECHOLAMINE CONTENT OF SINGLE MAMMALIAN VESICLES BY COLLISION–ADSORPTION EVENTS AT AN ELECTRODE. *JOURNAL OF THE AMERICAN CHEMICAL SOCIETY*, 137(13), 4344-4346.
44. NEHER, E. (2018). NEUROSECRETION: WHAT CAN WE LEARN FROM CHROMAFFIN CELLS. *PFLÜGERS ARCHIV-EUROPEAN JOURNAL OF PHYSIOLOGY*, 470(1), 7-11.
45. TISCHLER, A. S. (2002). CHROMAFFIN CELLS AS MODELS OF ENDOCRINE CELLS AND NEURONS. *ANNALS OF THE NEW YORK ACADEMY OF SCIENCES*, 971(1), 366-370.
46. GREENE, L. A., & TISCHLER, A. S. (1976). ESTABLISHMENT OF A NORADRENERGIC CLONAL LINE OF RAT ADRENAL PHEOCHROMOCYTOMA CELLS WHICH RESPOND TO NERVE GROWTH FACTOR. *PROCEEDINGS OF THE NATIONAL ACADEMY OF SCIENCES*, 73(7), 2424-2428.
47. COUPLAND, R. E. (1965). ELECTRON MICROSCOPIC OBSERVATIONS ON THE STRUCTURE OF THE RAT ADRENAL MEDULLA: I. THE ULTRASTRUCTURE AND ORGANIZATION OF CHROMAFFIN CELLS IN THE NORMAL ADRENAL MEDULLA. *JOURNAL OF ANATOMY*, 99(Pt 2), 231.
48. GREENE, L. A., & REIN, G. (1977). SYNTHESIS, STORAGE AND RELEASE OF ACETYLCHOLINE BY A NORADRENERGIC PHEOCHROMOCYTOMA CELL LINE. *NATURE*, 268(5618), 349-351.
49. JAHN, R., LANG, T., & SÜDHOF, T. C. (2003). MEMBRANE FUSION. *CELL*, 112(4), 519-533.
50. SÜDHOF, T. C., & ROTHMAN, J. E. (2009). MEMBRANE FUSION: GRAPPLING WITH SNARE AND SM PROTEINS. *SCIENCE*, 323(5913), 474-477.
51. SUTTON, R. B., FASSHAUER, D., JAHN, R., & BRUNGER, A. T. (1998). CRYSTAL STRUCTURE OF A SNARE COMPLEX INVOLVED IN SYNAPTIC EXOCYTOSIS AT 2.4 Å RESOLUTION. *NATURE*, 395(6700), 347-353.
52. BORISOVSKA, M., ZHAO, Y., TSYTSYURA, Y., GLYVUK, N., TAKAMORI, S., MATTI, U., ... & BRUNS, D. (2005). v-SNARES CONTROL EXOCYTOSIS OF VESICLES FROM PRIMING TO FUSION. *THE EMBO JOURNAL*, 24(12), 2114-2126.
53. PLATTNER, H., ARTALEJO, A. R., & NEHER, E. (1997). ULTRASTRUCTURAL ORGANIZATION OF BOVINE CHROMAFFIN CELL CORTEX—ANALYSIS BY CRYOFIXATION AND MORPHOMETRY OF ASPECTS PERTINENT TO EXOCYTOSIS. *THE JOURNAL OF CELL BIOLOGY*, 139(7), 1709-1717.
54. DUNEVALL, J., FATHALI, H., NAJAFINOBAR, N., LOVRIC, J., WIGSTRÖM, J., CANS, A. S., & EWING, A. G. (2015). CHARACTERIZING THE CATECHOLAMINE CONTENT OF SINGLE MAMMALIAN VESICLES BY COLLISION–ADSORPTION EVENTS AT AN ELECTRODE. *JOURNAL OF THE AMERICAN CHEMICAL SOCIETY*, 137(13), 4344-4346.
55. ALBILLOS, A., DERNICK, G., HORSTMANN, H., ALMERS, W., DE TOLEDO, G. A., & LINDAU, M. (1997). THE EXOCYTIC EVENT IN CHROMAFFIN CELLS REVEALED BY PATCH AMPEROMETRY. *NATURE*, 389(6650), 509-512.
56. WINKLER, H., & WESTHEAD, E. (1980). THE MOLECULAR ORGANIZATION OF ADRENAL CHROMAFFIN GRANULES. *NEUROSCIENCE*, 5(11), 1803-1823.
57. ESTÉVEZ-HERRERA, J., GONZÁLEZ-SANTANA, A., BAZ-DÁVILA, R., MACHADO, J. D., & BORGES, R. (2016). THE INTRAVESICULAR COCKTAIL AND ITS ROLE IN THE REGULATION OF EXOCYTOSIS. *JOURNAL OF NEUROCHEMISTRY*, 137(6), 897-903.
58. TERLAND, O., & FLATMARK, T. (1975). ASCORBATE AS A NATURAL CONSTITUENT OF CHROMAFFIN GRANULES FROM THE BOVINE ADRENAL MEDULLA. *FEBS LETTERS*, 59(1), 52-56.
59. SANTODOMINGO, J., VAY, L., CAMACHO, M., HERNÁNDEZ-SANMIGUEL, E., FONTERIZ, R. I., LOBATÓN, C. D., ... & ALVAREZ, J. (2008). CALCIUM DYNAMICS IN BOVINE ADRENAL MEDULLA CHROMAFFIN CELL SECRETORY GRANULES. *EUROPEAN JOURNAL OF NEUROSCIENCE*, 28(7), 1265-1274.

60. WIGHTMAN, R. M., DOMÍNGUEZ, N., & BORGES, R. (2018). HOW INTRAVESICULAR COMPOSITION AFFECTS EXOCYTOSIS. *PFLÜGERS ARCHIV-EUROPEAN JOURNAL OF PHYSIOLOGY*, 470(1), 135-141.
61. HILLARP, N. Å. (1960). CATECHOLAMINES: MECHANISMS OF STORAGE AND RELEASE. *ACTA ENDOCRINOLOGICA*, 34(2 SUPPLA), S181-S185.
62. HELLE, K. B., REED, R. K., PIHL, K. E., & SERCK-HANSSSEN, G. (1985). OSMOTIC PROPERTIES OF THE CHROMOGRANINS AND RELATION TO OSMOTIC PRESSURE IN CATECHOLAMINE STORAGE GRANULES. *ACTA PHYSIOLOGICA*, 123(1), 21-33.
63. KOPELL, W. N., & WESTHEAD, E. W. (1982). OSMOTIC PRESSURES OF SOLUTIONS OF ATP AND CATECHOLAMINES RELATING TO STORAGE IN CHROMAFFIN GRANULES. *JOURNAL OF BIOLOGICAL CHEMISTRY*, 257(10), 5707-5710.
64. YOO, S. H., & ALBANESI, J. P. (1990). CA<sup>2+</sup> (+)-INDUCED CONFORMATIONAL CHANGE AND AGGREGATION OF CHROMOGRANIN A. *JOURNAL OF BIOLOGICAL CHEMISTRY*, 265(24), 14414-14421.
65. DÍAZ-VERA, J., CAMACHO, M., MACHADO, J. D., DOMÍNGUEZ, N., MONTESINOS, M. S., HERNÁNDEZ-FERNAUD, J. R., ... & BORGES, R. (2012). CHROMOGRANINS A AND B ARE KEY PROTEINS IN AMINE ACCUMULATION, BUT THE CATECHOLAMINE SECRETORY PATHWAY IS CONSERVED WITHOUT THEM. *THE FASEB JOURNAL*, 26(1), 430-438.
66. GRANOT, J. (1978). NMR STUDIES OF CATECHOLAMINES. INTERACTIONS WITH ADENINE NUCLEOTIDES BY <sup>31</sup>P MAGNETIC RESONANCE. *FEBS LETTERS*, 88(2), 283-286.
67. GRANOT, J., & FIAT, D. (1977). NMR STUDIES OF CATECHOLAMINES. INTERACTIONS WITH ADENINE NUCLEOTIDES AND DIVALENT METAL IONS IN AQUEOUS SOLUTION. *JOURNAL OF THE AMERICAN CHEMICAL SOCIETY*, 99(15), 4963-4968.
68. WEDER, H. G., & WIEGAND, U. W. (1973). THE INTERACTION OF BIOGENIC AMINES WITH ADENOSINE-5'-TRIPHOSPHATE: A CALORIMETRIC STUDY. *FEBS LETTERS*, 38(1), 64-66.
69. TALEAT, Z., ESTÉVEZ-HERRERA, J., MACHADO, J. D., DUNEVALL, J., EWING, A. G., & BORGES, R. (2017). ELECTROCHEMICAL INVESTIGATION OF THE INTERACTION BETWEEN CATECHOLAMINES AND ATP. *ANALYTICAL CHEMISTRY*.
70. WINKLER, H. (1993). THE ADRENAL CHROMAFFIN GRANULE: A MODEL FOR LARGE DENSE CORE VESICLES OF ENDOCRINE AND NERVOUS TISSUE. *JOURNAL OF ANATOMY*, 183(Pt 2), 237.
71. TAKAMORI, S., HOLT, M., STENIUS, K., LEMKE, E. A., GRØNBORG, M., RIEDEL, D., ... & MÜLLER, S. A. (2006). MOLECULAR ANATOMY OF A TRAFFICKING ORGANELLE. *CELL*, 127(4), 831-846.
- NELSON, N., & HARVEY, W. R. (1999). VACUOLAR AND PLASMA MEMBRANE PROTON-ADENOSINETRIPHOSPHATASES. *PHYSIOLOGICAL REVIEWS*, 79(2), 361-385.
72. MIESENBOCK, G., DE ANGELIS, D. A., & ROTHMAN, J. E. (1998). VISUALIZING SECRETION AND SYNAPTIC TRANSMISSION WITH pH-SENSITIVE GREEN FLUORESCENT PROTEINS. *NATURE*, 394(6689), 192-195.
73. DÍAZ-VERA, J., MORALES, Y. G., HERNÁNDEZ-FERNAUD, J. R., CAMACHO, M., MONTESINOS, M. S., CALEGARI, F., ... & MACHADO, J. D. (2010). CHROMOGRANIN B GENE ABLATION REDUCES THE CATECHOLAMINE CARGO AND DECELERATES EXOCYTOSIS IN CHROMAFFIN SECRETORY VESICLES. *JOURNAL OF NEUROSCIENCE*, 30(3), 950-957.
74. HIASA, M., TOGAWA, N., & MORIYAMA, Y. (2014). VESICULAR NUCLEOTIDE TRANSPORT: A BRIEF HISTORY AND THE VESICULAR NUCLEOTIDE TRANSPORTER AS A TARGET FOR DRUG DEVELOPMENT. *CURRENT PHARMACEUTICAL DESIGN*, 20(16), 2745-2749.
75. HENRY, J. P., SAGNÉ, C., BEDET, C., & GASNIER, B. (1998). THE VESICULAR MONOAMINE TRANSPORTER: FROM CHROMAFFIN GRANULE TO BRAIN. *NEUROCHEMISTRY INTERNATIONAL*, 32(3), 227-246.
76. GASNIER, B. (2000). THE LOADING OF NEUROTRANSMITTERS INTO SYNAPTIC VESICLES. *BIOCHIMIE*, 82(4), 327-337.
77. COLLIVER, T. L., PYOTT, S. J., ACHALABUN, M., & EWING, A. G. (2000). VMAT-MEDIATED CHANGES IN QUANTAL SIZE AND VESICULAR VOLUME. *JOURNAL OF NEUROSCIENCE*, 20(14), 5276-5282.
78. OLEINICK, A., HU, R., REN, B., TIAN, Z. Q., SVIR, I., & AMATORE, C. (2016). THEORETICAL MODEL OF NEUROTRANSMITTER RELEASE DURING IN VIVO VESICULAR EXOCYTOSIS BASED ON A GRAINY BIPHASIC NANO-STRUCTURATION OF CHROMOGRANINS WITHIN DENSE CORE MATRIXES. *JOURNAL OF THE ELECTROCHEMICAL SOCIETY*, 163(4), H3014-H3024.
79. REN, L., MELLANDER, L. J., KEIGHRON, J., CANS, A. S., KURCZY, M. E., SVIR, I., ... & EWING, A. G. (2016). THE EVIDENCE FOR OPEN AND CLOSED EXOCYTOSIS AS THE PRIMARY RELEASE MECHANISM. *QUARTERLY REVIEWS OF BIOPHYSICS*, 49.
80. FESCE, R., GROHOVAZ, F., VALTORTA, F., & MELDOLESI, J. (1994). NEUROTRANSMITTER RELEASE: FUSION OR 'KISS-AND-RUN'? *TRENDS IN CELL BIOLOGY*, 4(1), 1-4.
81. ALBILLOS, A., DERNICK, G., HORSTMANN, H., ALMERS, W., DE TOLEDO, G. A., & LINDAU, M. (1997). THE EXOCYTIC EVENT IN CHROMAFFIN CELLS REVEALED BY PATCH AMPEROMETRY. *NATURE*, 389(6650), 509-512.

82. ARTALEJO, C. R., ELHAMDANI, A., & PALFREY, H. C. (1998). SECRETION: DENSE-CORE VESICLES CAN KISS-AND-RUN TOO. *CURRENT BIOLOGY*, 8(2), R62-R65.
83. OMIATEK, D. M., DONG, Y., HEIEN, M. L., & EWING, A. G. (2010). ONLY A FRACTION OF QUANTAL CONTENT IS RELEASED DURING EXOCYTOSIS AS REVEALED BY ELECTROCHEMICAL CYTOMETRY OF SECRETORY VESICLES. *ACS CHEMICAL NEUROSCIENCE*, 1(3), 234-245.
84. MELLANDER, L. J., TROUILLON, R., SVENSSON, M. I., & EWING, A. G. (2012). AMPEROMETRIC POST SPIKE FEET REVEAL MOST EXOCYTOSIS IS VIA EXTENDED KISS-AND-RUN FUSION. *SCIENTIFIC REPORTS*, 2, 907.
85. AMATORE, C., OLEINICK, A. I., & SVIR, I. (2010). RECONSTRUCTION OF APERTURE FUNCTIONS DURING FULL FUSION IN VESICULAR EXOCYTOSIS OF NEUROTRANSMITTERS. *CHEMPHYSCHEM*, 11(1), 159-174.
86. STAAL, R. G., MOSHAROV, E. V., & SULZER, D. (2004). DOPAMINE NEURONS RELEASE TRANSMITTER VIA A FLICKERING FUSION PORE. *NATURE NEUROSCIENCE*, 7(4), 341-346.
87. MAJDI, S., BERGLUND, E. C., DUNEVALL, J., OLEINICK, A. I., AMATORE, C., KRANTZ, D. E., & EWING, A. G. (2015). ELECTROCHEMICAL MEASUREMENTS OF OPTOGENETICALLY STIMULATED QUANTAL AMINE RELEASE FROM SINGLE NERVE CELL VARICOSITIES IN DROSOPHILA LARVAE. *ANGEWANDTE CHEMIE*, 127(46), 13813-13816.
88. ALÉS, E., TABARES, L., POYATO, J. M., VALERO, V., LINDAU, M., & DE TOLEDO, G. A. (1999). HIGH CALCIUM CONCENTRATIONS SHIFT THE MODE OF EXOCYTOSIS TO THE KISS-AND-RUN MECHANISM. *NATURE CELL BIOLOGY*, 1(1), 40-44.
89. ELHAMDANI, A., PALFREY, H. C., & ARTALEJO, C. R. (2001). QUANTAL SIZE IS DEPENDENT ON STIMULATION FREQUENCY AND CALCIUM ENTRY IN CALF CHROMAFFIN CELLS. *NEURON*, 31(5), 819-830.
90. DOREIAN, B. W., FULOP, T. G., & SMITH, C. B. (2008). MYOSIN II ACTIVATION AND ACTIN REORGANIZATION REGULATE THE MODE OF QUANTAL EXOCYTOSIS IN MOUSE ADRENAL CHROMAFFIN CELLS. *JOURNAL OF NEUROSCIENCE*, 28(17), 4470-4478.
91. FULOP, T., & SMITH, C. (2007). MATCHING NATIVE ELECTRICAL STIMULATION BY GRADED CHEMICAL STIMULATION IN ISOLATED MOUSE ADRENAL CHROMAFFIN CELLS. *JOURNAL OF NEUROSCIENCE METHODS*, 166(2), 195-202.
92. TROUILLON, R., & EWING, A. G. (2014). ACTIN CONTROLS THE VESICULAR FRACTION OF DOPAMINE RELEASED DURING EXTENDED KISS AND RUN EXOCYTOSIS. *ACS CHEMICAL BIOLOGY*, 9(3), 812-820.
93. WIERDA, K. D., TOONEN, R. F., DE WIT, H., BRUSSAARD, A. B., & VERHAGE, M. (2007). INTERDEPENDENCE OF PKC-DEPENDENT AND PKC-INDEPENDENT PATHWAYS FOR PRESYNAPTIC PLASTICITY. *NEURON*, 54(2), 275-290.
94. VOETS, T., TOONEN, R. F., BRIAN, E. C., DE WIT, H., MOSER, T., RETTIG, J., ... & VERHAGE, M. (2001). MUNC18-1 PROMOTES LARGE DENSE-CORE VESICLE DOCKING. *NEURON*, 31(4), 581-592.
95. ÑECO, P., GINER, D., VINIEGRA, S., BORGES, R., VILLARROEL, A., & GUTIÉRREZ, L. M. (2004). NEW ROLES OF MYOSIN II DURING VESICLE TRANSPORT AND FUSION IN CHROMAFFIN CELLS. *JOURNAL OF BIOLOGICAL CHEMISTRY*, 279(26), 27450-27457.
96. MACHADO, J. D., MORALES, A., GOMEZ, J. F., & BORGES, R. (2001). cAMP MODULATES EXOCYTOTIC KINETICS AND INCREASES QUANTAL SIZE IN CHROMAFFIN CELLS. *MOLECULAR PHARMACOLOGY*, 60(3), 514-520.
97. UCHIYAMA, Y., MAXSON, M. M., SAWADA, T., NAKANO, A., & EWING, A. G. (2007). PHOSPHOLIPID MEDIATED PLASTICITY IN EXOCYTOSIS OBSERVED IN PC12 CELLS. *BRAIN RESEARCH*, 1151, 46-54.
98. AMATORE, C., ARBAULT, S., BONIFAS, I., BOURET, Y., ERARD, M., & GUILLE, M. (2003). DYNAMICS OF FULL FUSION DURING VESICULAR EXOCYTOTIC EVENTS: RELEASE OF ADRENALINE BY CHROMAFFIN CELLS. *CHEMPHYSCHEM*, 4(2), 147-154.
99. CHURCHWARD, M. A., & COORSSEN, J. R. (2009). CHOLESTEROL, REGULATED EXOCYTOSIS AND THE PHYSIOLOGICAL FUSION MACHINE. *BIOCHEMICAL JOURNAL*, 423(1), 1-14.
100. NAJAFINOBAR, N., MELLANDER, L. J., KURCZY, M. E., DUNEVALL, J., ANGERER, T. B., FLETCHER, J. S., & CANS, A. S. (2016). CHOLESTEROL ALTERS THE DYNAMICS OF RELEASE IN PROTEIN INDEPENDENT CELL MODELS FOR EXOCYTOSIS. *SCIENTIFIC REPORTS*, 6, 33702.
101. LANG, T., BRUNS, D., WENZEL, D., RIEDEL, D., HOLROYD, P., THIELE, C., & JAHN, R. (2001). SNAREs ARE CONCENTRATED IN CHOLESTEROL-DEPENDENT CLUSTERS THAT DEFINE DOCKING AND FUSION SITES FOR EXOCYTOSIS. *THE EMBO JOURNAL*, 20(9), 2202-2213.
102. SHARMA, S., & LINDAU, M. (2017). T-SNARE TRANSMEMBRANE DOMAIN CLUSTERING MODULATES LIPID ORGANIZATION AND MEMBRANE CURVATURE. *JOURNAL OF THE AMERICAN CHEMICAL SOCIETY*.

103. HU, R., REN, B., LIN, C. J., OLEINICK, A., SVIR, I., TIAN, Z. Q., & AMATORE, C. (2016). HOW "FULL" IS "FULL FUSION" DURING EXOCYTOSIS FROM DENSE CORE VESICLES? EFFECT OF SDS ON "QUANTAL" RELEASE AND FINAL FUSION PORE SIZE. *JOURNAL OF THE ELECTROCHEMICAL SOCIETY*, 163(9), H853-H865.
104. MAJDI, S., NAJAFINOBAR, N., DUNEVALL, J., LOVRIC, J., & EWING, A. G. (2017). DMSO CHEMICALLY ALTERS CELL MEMBRANES TO SLOW EXOCYTOSIS AND INCREASE THE FRACTION OF PARTIAL TRANSMITTER RELEASED. *CHEMBIOCHEM*, 18(19), 1898-1902.
105. TROUILLON, R., & EWING, A. G. (2013). AMPEROMETRIC MEASUREMENTS AT CELLS SUPPORT A ROLE FOR DYNAMIN IN THE DILATION OF THE FUSION PORE DURING EXOCYTOSIS. *CHEMPHYSCHEM*, 14(10), 2295-2301.
106. BARD, A. J., FAULKNER, L. R., LEDDY, J., & ZOSKI, C. G. (1980). *ELECTROCHEMICAL METHODS: FUNDAMENTALS AND APPLICATIONS (VOL. 2)*. NEW YORK: WILEY.
107. SHOUP, D., & SZABO, A. (1982). CHRONOAMPEROMETRIC CURRENT AT FINITE DISK ELECTRODES. *JOURNAL OF ELECTROANALYTICAL CHEMISTRY AND INTERFACIAL ELECTROCHEMISTRY*, 140(2), 237-245.
108. AOKI, K., & OSTERYOUNG, J. (1981). DIFFUSION-CONTROLLED CURRENT AT THE STATIONARY FINITE DISK ELECTRODE: THEORY. *JOURNAL OF ELECTROANALYTICAL CHEMISTRY AND INTERFACIAL ELECTROCHEMISTRY*, 122, 19-35.
109. AOKI, K., & OSTERYOUNG, J. (1981). DIFFUSION CONTROLLED CURRENT AT A STATIONARY FINITE DISK ELECTRODE: EXPERIMENT. *JOURNAL OF ELECTROANALYTICAL CHEMISTRY AND INTERFACIAL ELECTROCHEMISTRY*, 125(2), 315-320.
110. OLDHAM, K. B. (1979). ANALYTICAL EXPRESSIONS FOR THE REVERSIBLE RANDLES-SEVCIK FUNCTION. *JOURNAL OF ELECTROANALYTICAL CHEMISTRY AND INTERFACIAL ELECTROCHEMISTRY*, 105(2), 373-375.
111. SCHOLZ, F. (2010). *ELECTROANALYTICAL METHODS (VOL. 1)*. BERLIN-HEIDELBERG: SPRINGER.
112. ADAMS, R. (1958). CARBON PASTE ELECTRODES. *ANALYTICAL CHEMISTRY*, 30(9), 1576-1576
113. OLSON, C., & ADAMS, R. N. (1960). CARBON PASTE ELECTRODES APPLICATION TO ANODIC VOLTAMMETRY. *ANALYTICA CHIMICA ACTA*, 22, 582-589.
114. ADAMS, R. N. (1969). ANODIC OXIDATION PATHWAYS OF AROMATIC HYDROCARBONS AND AMINES. *ACCOUNTS OF CHEMICAL RESEARCH*, 2(6), 175-180.
115. HAWLEY, M. D., TATAWAWADI, S. V., PIEKARSKI, S., & ADAMS, R. N. (1967). ELECTROCHEMICAL STUDIES OF THE OXIDATION PATHWAYS OF CATECHOLAMINES. *JOURNAL OF THE AMERICAN CHEMICAL SOCIETY*, 89(2), 447-450.
116. ADAMS, R. N. (1969). APPLICATIONS OF MODERN ELECTROANALYTICAL TECHNIQUES TO PHARMACEUTICAL CHEMISTRY. *JOURNAL OF PHARMACEUTICAL SCIENCES*, 58(10), 1171-1184.
117. KISSINGER, P. T., HART, J. B., & ADAMS, R. N. (1973). VOLTAMMETRY IN BRAIN TISSUE—A NEW NEUROPHYSIOLOGICAL MEASUREMENT. *BRAIN RESEARCH*, 55(1), 209-213.
118. BICHER, H. I., & KNISELY, M. H. (1970). BRAIN TISSUE REOXYGENATION TIME, DEMONSTRATED WITH A NEW ULTRAMICRO OXYGEN ELECTRODE. *JOURNAL OF APPLIED PHYSIOLOGY*, 28(3), 387-390.
119. KORYTA, J., PRADÁČ, J., PRADÁČOVÁ, J., & OSSENDORFOVA, N. (1971). ORGANIC OXIDATION-REDUCTION SYSTEMS AS ELECTROCHEMICAL INDICATORS FOR MONITORING IN ORGANS IN VIVO. IN *BIOLOGICAL ASPECTS OF ELECTROCHEMISTRY* (PP. 367-373). BIRKHÄUSER BASEL.
120. PRADÁČ, J., PRADÁČOVÁ, J., & KORYTA, J. (1971). CYCLIC-VOLTAMMETRIC DETERMINATION OF CYSTEINE IN RAT ORGANS AFTER INTRAVENOUS INJECTION. *BIOCHIMICA ET BIOPHYSICA ACTA (BBA)-GENERAL SUBJECTS*, 237(3), 450-454.
121. MCCREERY, R. L., DREILING, R., & ADAMS, R. N. (1974). VOLTAMMETRY IN BRAIN TISSUE: THE FATE OF INJECTED 6-HYDROXYDOPAMINE. *BRAIN RESEARCH*, 73(1), 15-21.
122. MCCREERY, R. L., DREILING, R., & ADAMS, R. N. (1974). VOLTAMMETRY IN BRAIN TISSUE: QUANTITATIVE STUDIES OF DRUG INTERACTIONS. *BRAIN RESEARCH*, 73(1), 23-33.
123. CONTI, J. C., STROPE, E., ADAMS, R. N., & MARSDEN, C. A. (1978). VOLTAMMETRY IN BRAIN TISSUE: CHRONIC RECORDING OF STIMULATED DOPAMINE AND 5-HYDROXYTRYPTAMINE RELEASE. *LIFE SCIENCES*, 23(27-28), 2705-2715.

124. LINDSAY, W. S., KIZZORT, B. L., JUSTICE, J. B., SALAMONE, J. D., & NEILL, D. B. (1980). AN AUTOMATED ELECTROCHEMICAL METHOD FOR IN VIVO MONITORING OF CATECHOLAMINE RELEASE. *JOURNAL OF NEUROSCIENCE METHODS*, 2(4), 373-388.
125. LANE, R. F., HUBBARD, A. T., & BLAHA, C. D. (1978). 243-BRAIN DOPAMINERGIC NEURONS: IN VIVO ELECTROCHEMICAL INFORMATION CONCERNING STORAGE, METABOLISM AND RELEASE PROCESSES. *BIOELECTROCHEMISTRY AND BIOENERGETICS*, 5(3), 504-525.
126. LANE, R. F., HUBBARD, A. T., FUKUNAGA, K., & BLANCHARD, R. J. (1976). BRAIN CATECHOLAMINES: DETECTION IN VIVO BY MEANS OF DIFFERENTIAL PULSE VOLTAMMETRY AT SURFACE-MODIFIED PLATINUM ELECTRODES. *BRAIN RESEARCH*, 114(2), 346-352.
127. JENNINGS, V. J., & PEARSON, P. (1975). CARBON FIBRE PH-SENSITIVE ELECTRODE. *NATURE*, 256(5512), 31-31.
128. ELLIS, D., & THOMAS, R. C. (1976). MICROELECTRODE MEASUREMENT OF THE INTRACELLULAR PH OF MAMMALIAN HEART CELLS. *NATURE*, 262(5565), 224-225.
129. AICKIN, C. C., & THOMAS, R. C. (1975). MICRO-ELECTRODE MEASUREMENT OF THE INTERNAL PH OF CRAB MUSCLE FIBRES. *THE JOURNAL OF PHYSIOLOGY*, 252(3), 803-815.
130. PONCHON, J. L., CESPUGLIO, R., GONON, F., JOUVET, M., & PUJOL, J. F. (1979). NORMAL PULSE POLAROGRAPHY WITH CARBON FIBER ELECTRODES FOR IN VITRO AND IN VIVO DETERMINATION OF CATECHOLAMINES. *ANALYTICAL CHEMISTRY*, 51(9), 1483-1486.
131. ARMSTRONG-JAMES, M., & MILLAR, J. (1979). CARBON FIBRE MICROELECTRODES. *JOURNAL OF NEUROSCIENCE METHODS*, 1(3), 279-287.
132. FOX, K., ARMSTRONG-JAMES, M., & MILLAR, J. (1980). THE ELECTRICAL CHARACTERISTICS OF CARBON FIBRE MICROELECTRODES. *JOURNAL OF NEUROSCIENCE METHODS*, 3(1), 37-48.
133. DAYTON, M. A., BROWN, J. C., STUTTS, K. J., & WIGHTMAN, R. M. (1980). FARADAIC ELECTROCHEMISTRY AT MICROVOLTAMMETRIC ELECTRODES. *ANALYTICAL CHEMISTRY*, 52(6), 946-950.
134. KRUK, Z. L., ARMSTRONG-JAMES, M., & MILLAR, J. (1980). MEASUREMENT OF THE CONCENTRATION OF 5-HYDROXYTRYPTAMINE EJECTED DURING IONTOPHORESIS USING MULTIBARREL CARBON FIBRE MICROELECTRODES. *LIFE SCIENCES*, 27(22), 2093-2098.
135. GONON, F., BUDA, M., CESPUGLIO, R., JOUVET, M., & PUJOL, J. F. (1980). IN VIVO ELECTROCHEMICAL DETECTION OF CATECHOLS IN THE NEOSTRIATUM OF ANAESTHETIZED RATS: DOPAMINE OR DOPAC?. *NATURE*, 286(5776), 902.
136. GONON, F., BUDA, M., CESPUGLIO, R., & JOUVET, M. (1981). VOLTAMMETRY IN THE STRIATUM OF CHRONIC FREELY MOVING RATS: DETECTION OF CATECHOLS AND ASCORBIC ACID. *BRAIN RESEARCH*, 223(1), 69-80.
137. CESPUGLIO, R., FARADJI, H., PONCHON, J. L., BUDA, M., RIOU, F., GONON, F., ... & JOUVET, M. (1981). DIFFERENTIAL PULSE VOLTAMMETRY IN BRAIN TISSUE. I. DETECTION OF 5-HYDROXYINDOLES IN THE RAT STRIATUM. *BRAIN RESEARCH*, 223(2), 287-298.
138. CESPUGLIO, R., FARADJI, H., RIOU, F., BUDA, M., GONON, F., PUJOL, J. F., & JOUVET, M. (1981). DIFFERENTIAL PULSE VOLTAMMETRY IN BRAIN TISSUE. II. DETECTION OF 5-HYDROXYINDOLACETIC ACID IN THE RAT STRIATUM. *BRAIN RESEARCH*, 223(2), 299-311.
139. EWING, A. G., BIGELOW, J. C., & WIGHTMAN, R. M. (1983). DIRECT IN VIVO MONITORING OF DOPAMINE RELEASED FROM TWO STRIATAL COMPARTMENTS IN THE RAT. *SCIENCE*, 221(4606), 169-171.
140. LESZCZYNSKY, D. J., JANKOWSKI, J. A., VIVEROS, O. H., DILIBERTO, E. J., NEAR, J. A., & WIGHTMAN, R. M. (1990). NICOTINIC RECEPTOR-MEDIATED CATECHOLAMINE SECRETION FROM INDIVIDUAL CHROMAFFIN CELLS. CHEMICAL EVIDENCE FOR EXOCYTOSIS. *JOURNAL OF BIOLOGICAL CHEMISTRY*, 265(25), 14736-14737.



158. CHALFIE, M., TU, Y., EUSKIRCHEN, G., WARD, W. W., & PRASHER, D. C. (1994). GREEN FLUORESCENT PROTEIN AS A MARKER FOR GENE EXPRESSION. *SCIENCE*, 802-805.
159. HEIM, R., PRASHER, D. C., & TSIEN, R. Y. (1994). WAVELENGTH MUTATIONS AND POSTTRANSLATIONAL AUTOXIDATION OF GREEN FLUORESCENT PROTEIN. *PROCEEDINGS OF THE NATIONAL ACADEMY OF SCIENCES*, 91(26), 12501-12504.
160. HEIM, R., CUBBITT, A. B., & TSIEN, R. Y. (1995). IMPROVED GREEN FLUORESCENCE. *NATURE*, 373(6516), 663-664.
161. CUBBITT, A. B., HEIM, R., ADAMS, S. R., BOYD, A. E., GROSS, L. A., & TSIEN, R. Y. (1995). UNDERSTANDING, IMPROVING AND USING GREEN FLUORESCENT PROTEINS. *TRENDS IN BIOCHEMICAL SCIENCES*, 20(11), 448-455.
162. TSIEN, R. Y. (1998). THE GREEN FLUORESCENT PROTEIN.
163. KREMERS, G. J., GILBERT, S. G., CRANFILL, P. J., DAVIDSON, M. W., & PISTON, D. W. (2011). FLUORESCENT PROTEINS AT A GLANCE. *J CELL SCI*, 124(2), 157-160.
164. GUBERNATOR, N. G., ZHANG, H., STAAL, R. G., MOSHAROV, E. V., PEREIRA, D. B., YUE, M., ... & SULZER, D. (2009). FLUORESCENT FALSE NEUROTRANSMITTERS VISUALIZE DOPAMINE RELEASE FROM INDIVIDUAL PRESYNAPTIC TERMINALS. *SCIENCE*, 324(5933), 1441-1444.
165. HU, G., HENKE, A., KARPOWICZ JR, R. J., SONDEERS, M. S., FARRIMOND, F., EDWARDS, R., ... & SAMES, D. (2013). NEW FLUORESCENT SUBSTRATE ENABLES QUANTITATIVE AND HIGH-THROUGHPUT EXAMINATION OF VESICULAR MONOAMINE TRANSPORTER 2 (VMAT2). *ACS CHEMICAL BIOLOGY*, 8(9), 1947-1954.
166. LEE, M., GUBERNATOR, N. G., SULZER, D., & SAMES, D. (2010). DEVELOPMENT OF PH-RESPONSIVE FLUORESCENT FALSE NEUROTRANSMITTERS. *JOURNAL OF THE AMERICAN CHEMICAL SOCIETY*, 132(26), 8828-8830.
167. AXELROD, D. (2001). TOTAL INTERNAL REFLECTION FLUORESCENCE MICROSCOPY IN CELL BIOLOGY. *TRAFFIC*, 2(11), 764-774.
168. STEYER, J. A., & ALMERS, W. (1999). TRACKING SINGLE SECRETORY GRANULES IN LIVE CHROMAFFIN CELLS BY EVANESCENT-FIELD FLUORESCENCE MICROSCOPY. *BIOPHYSICAL JOURNAL*, 76(4), 2262-2271.
169. TSUBOI, T., & RUTTER, G. A. (2003). MULTIPLE FORMS OF "KISS-AND-RUN" EXOCYTOSIS REVEALED BY EVANESCENT WAVE MICROSCOPY. *CURRENT BIOLOGY*, 13(7), 563-567.
170. KHOSHOUEI, M., RADJAINIA, M., BAUMEISTER, W., & DANEV, R. (2016). CRYO-EM STRUCTURE OF HAEMOGLOBIN AT 3.2 Å DETERMINED WITH THE VOLTA PHASE PLATE. *BIORXIV*, 087841.
171. HANRIEDER, J., MALMBERG, P., & EWING, A. G. (2015). SPATIAL NEUROPROTEOMICS USING IMAGING MASS SPECTROMETRY. *BIOCHIMICA ET BIOPHYSICA ACTA (BBA)-PROTEINS AND PROTEOMICS*, 1854(7), 718-731.
172. CAPRIOLI, R. M., FARMER, T. B., & GILE, J. (1997). MOLECULAR IMAGING OF BIOLOGICAL SAMPLES: LOCALIZATION OF PEPTIDES AND PROTEINS USING MALDI-TOF MS. *ANALYTICAL CHEMISTRY*, 69(23), 4751-4760
173. KAYA, I., BRINET, D., MICHNO, W., BAŞKURT, M., ZETTERBERG, H., BLENOW, K., & HANRIEDER, J. (2017). NOVEL TRIMODAL MALDI IMAGING MASS SPECTROMETRY (IMS3) AT 10 MM REVEALS SPATIAL LIPID AND PEPTIDE CORRELATES IMPLICATED IN AB PLAQUE PATHOLOGY IN ALZHEIMER'S DISEASE. *ACS CHEMICAL NEUROSCIENCE*, 8(12), 2778-2790.
174. ANGERER, T. B., BLENKINSOPP, P., & FLETCHER, J. S. (2015). HIGH ENERGY GAS CLUSTER IONS FOR ORGANIC AND BIOLOGICAL ANALYSIS BY TIME-OF-FLIGHT SECONDARY ION MASS SPECTROMETRY. *INTERNATIONAL JOURNAL OF MASS SPECTROMETRY*, 377, 591-598.
175. VICKERMAN, J. C., & BRIGGS, D. (Eds.). (2001). TOF-SIMS: SURFACE ANALYSIS BY MASS SPECTROMETRY. IM.
176. LOVRIĆ, J., DUNEVALL, J., LARSSON, A., REN, L., ANDERSSON, S., MEIBOM, A., ... & EWING, A. G. (2016). NANO SECONDARY ION MASS SPECTROMETRY IMAGING OF DOPAMINE DISTRIBUTION ACROSS NANOMETER VESICLES. *ACS NANO*, 11(4), 3446-3455.
177. DHATT, G., LEFRANÇOIS, E., & TOUZOT, G. (2012). FINITE ELEMENT METHOD. JOHN WILEY & SONS.